Reviews on Advanced Materials and Technologies, 2025, vol. 7, no. 4, pp. 222–258
DOI: 10.17586/2687-0568-2025-7-4-222-258

Computational Analysis of SiC Crystal Growth from Silicon Melt Diluted with Cr, Fe, Co, Ni, Y, Al, La, Ce, Pr, Nd, and Sc. Part 2

Andrei N. Vorob'ev [1,2]

[1] STR Group, Inc. – Soft-Impact, Ltd., Office 603, Bol'shoy Sampsonievskiy pr., 64, lit. E, St. Petersburg, 194044, Russia
[2] Sci-Tech Center "Glass and Ceramics", Ltd., Dudko 3, St. Petersburg, 192029, Russia

Article history

Received November 10, 2025
Received in revised form,
December 07, 2025
Accepted December 15, 2025
Available online December 23, 2025

Abstract

In consideration of experience gained in the previous research, an extended two-dimensional analysis of silicon carbide top-seeded solution growth is computationally carried out for 11 binary systems under conditions typical for the real process at temperature and composition varying in a wide range. Along with averaged values of the growth rate, its radial distribution over the seed is investigated for estimating the crystal surface shape. It is found that with the exception of aluminum the addition of other dopants to the silicon melt manifests itself through the growth rate saturation at their certain level above which the growth rate cannot be raised. As it follows from radial distributions obtained, their deviation from a convex parabolic profile decreases with co-solvent content and seed temperature. In this connection, chromium, lanthanides and yttrium can be distinguished as most promising dopants. Additionally, such ternary solutions as Si-Cr-Y and Si-La-Y are predicted to provide both relatively high growth rate and smooth surface of crystal at moderate doping.

Keywords: SiC growth; Silicon melt; Solution; Carbon solubility; CGSim (crystal growth simulation)

1. INTRODUCTION

The present paper is a logical continuation of the previous work [1] where the silicon carbide (SiC) top-seeded solution growth (TSSG) is computationally analyzed within a simplified approach. SiC TSSG method was described in Ref. [1]. Its main points are listed below.

First of all, it should be noted that SiC is reckoned to be one of most desirable materials for high-power and high-performance electronic devices. In this connection, SiC substrate plays an important role and can replace Si substrate in such applications due to its superior electric and thermal properties [2]. Until recently, SiC wafers are mostly fabricated by physical vapor transport (PVT) [3,4] but their high defect densities are formidable problems in making high-power electric devices.

Lately, SiC TSSG is drawing attention as an alternative method to grow high-quality SiC crystals [5]. The process concept is transparent: high-purity silicon melts in a graphite crucible while the carbon dissolves from the crucible to the melt, travels to the crystal surface and contributes to crystal growth [6,7]. The method has a huge advantage in reducing the dislocation density in the crystal by converting and eliminating the threading screw and edge dislocations [8,9]. This is associated with supposition that the growth proceeds under conditions close to the thermal equilibrium.

Nevertheless, SiC TSSG is seriously limited by low growth rate and low uniformity of the grown crystal due to low carbon solubility in the molten Si [10] and complicated fluid flow in the melt [11,12]. The carbon solubility can be enhanced by adding some metals into the melt [13,14]. As it is reported in Ref. [15], a high quality SiC has been obtained by TSSG technique using Si-Ti solution. In addition, SiC bulk crystal with 12 mm length has been grown using Si-Cr-based solution [16]. One of recent papers informs that to date 4-inch substrates with a thickness of 15 mm produced by solution growth have

* Corresponding author: Andrei N.Vorob'ev, e-mail: andrei.vorobiev@str-soft.com

been unveiled while substrates of 6 inches and above are still under development [17]. Thus, currently solution growth techniques are still in the research and development stage; however, they show promising potential for growing high-quality SiC crystals.

The previous paper [1] considers the effect of 11 additives to silicon melt on SiC growth rate and distinguishes most promising among them within simplified 0D-approach.

The goal of the present paper is to analyze the results of 2D-computations under real process conditions and to collate the influence of several co-solvents on both growth rate value and its radial distribution or uniformity over the seed surface. From the investigations, two ternary solutions are suggested, facilitating both relatively high growth rate and its minimum deviation from convex near-parabolic profile.

2. 2D-COMPUTATIONAL ANALYSIS

2.1. Averaged growth rate in binary solutions Si-Me, Me = Cr, Fe, Co, Ni, Y, Al, La, Ce, Pr, Nd and Sc

Two examples of 2D-simulation of SiC TSSG were presented in the previous paper [1] (see Section 3). Their demonstration aimed to give more extended and real information on inherent features and advantages of processes in using different co-solvents as compared with estimates obtained within the simplified 0D-approach (see Section 2.4 in Ref. [1]). Some important details of 2D-approach are considered below.

Modeling analog of the reactor with the seed diameter of 18 mm is employed for 2D-computations by CGSim software developed in STR Group [18]. Such rather small dimensions allow neglecting a flow turbulence that is supported by a criterion suggested in Ref. [19] and confining oneself to the consideration of molecular heat and mass transport. Then all thermophysical properties reviewed and collected in Ref. [1] are usable for 2D-computations without modification.

As mentioned in Ref. [1], the process temperature is normally controlled by measuring it in some points of the investigated set-up. In the case considered, they are centrally located above the SiC seed and under the bottom of graphite crucible acting as the carbon source (see Fig. 7 in Ref. [1]). Just CGSim [18] is suitable for tuning up the power of inductive heater in such a way as to provide the target temperatures at the controlled points. Obviously, the 2D-distribution of temperature turns out to be more complicated and non-uniform along the seed surface than that within the simplified approach [1]. Therefore, the temperature drop between the seed and the carbon source can deviate significantly from that between the controlled points, depending on the investigated solution and its composition as well as on the reactor design and the thermophysical properties of used materials.

The listed features are specific for each process and reactor design which should be accounted for when analyzing within 2D-computations by CGSim [18]. In the present paper, for comparing the modeling results to each other, they are obtained for the same set-up considered in Ref. [1].

To get a preliminary view of the growth rate in whole, its value averaged over the seed surface is illustrated in Fig. 1 as a function of composition at the temperature drop of 10 K and at the top temperature of 2000, 2100, 2200 and 2300 K. The co-solvent concentration range is limited by 80% since its higher percentage can cause its crucial penetration into the crystal. As seen from the plots, the growth rate rises with temperature. This trend manifests itself most clearly for silicon melt diluted with lanthanides (purple curves). Among them a maximum growth rate is predicted when applying the praseodymium (dashed dot purple). Lanthanum (solid purple) and cerium (dashed dot dot purple) provide a similar dependence of the growth rate which is lower than that at Pr-doping and considerably higher than that at Nd-addition (long dashed purple). In all cases above, the SiC growth rate peaks at a certain mole fraction of co-solvent and can no longer be raised by elevating the doping and then falls down. Particularly, a sharp maximum can be observed for Pr, La and Ce at high temperatures while it is less pronounced at Nd. Hence one can suppose that the percentage of listed co-solvents higher than 40–50 mol.% has a reverse effect. Additionally, the onset of growth rate saturation occurs at a lower doping concentration when using a higher process temperature.

The growth rate in Si-Cr solution (solid red) is predicted to reach its maximum of ≈ 100 μm/h at 2000 K and of ≈ 300 μm/h at 2300 K. This is essentially lower than the values obtained for lanthanides. Note that Cr-content at which the growth rate is saturated shifts from 50 to 40% in temperature range above.

The doping of silicon melt by yttrium (dashed red) gives ≈ 50 μm/h at 2000 K and at 30% Y and ≈ 170 μm/h at 2300 K and at 25% Y. It means that the growth rate can be increased by the least percentage of yttrium in spite of its low level in comparison with that provided by other co-solvents.

The addition of Fe (dashed dot dot red), Co (dashed dot red) and Ni (long dashed red) manifests itself only at their elevated concentration beginning with 60–70% whereas the maximum growth rate does not exceed the values reached at lanthanides and chromium. This makes them less preferable in use.

Si-Sc application (solid black) leads to the growth rate even lower than that in the pure silicon melt at moderate dilution. Its remarkable values can be observed at temperatures and Sc contents higher than 2200 K and 45%,

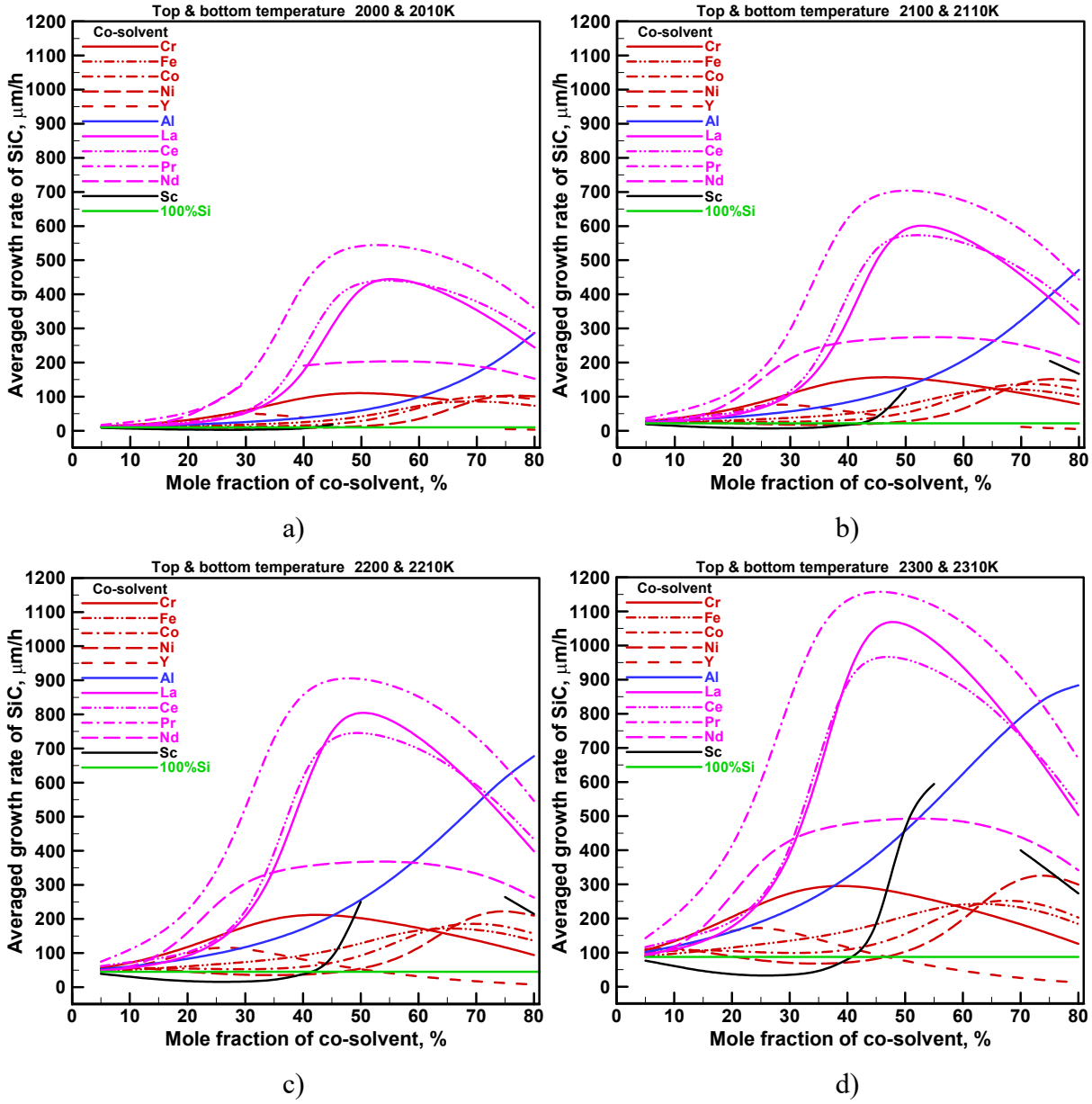

Fig. 1. Averaged growth rate in binary solutions vs co-solvent percentage at top temperature of 2000, 2100, 2200 and 2300 K.

respectively. However, the solidus-liquidus of Si-Sc system imposes some considerable constraints on using this solution at temperatures lower than 2300 K and at Sc content higher than 50%. It is shown by a discontinuity in the curve of the growth rate in Fig. 1.

With the exception of 2300 K (see Fig. 1d), a monotonic dependence of the growth rate is predicted for Al-doping. Its averaged values are close to those computed for Y when their percentage is lower than 25% and the temperature is about 2300 K. Note that the growth rate in Si-Al solution does not exceed that reached in Si-Nd at a reasonable content (< 50%).

Some general conclusions can be drawn from the analysis of the averaged growth rate:

– it rises with the process temperature for all studied solutions;

– with the exception of aluminum, an addition of other dopants results in its saturation at their certain percentage;

– its maximum slightly shifts to the left at elevated temperatures;

– its highest values are predicted for lanthanides.

Such results are in good agreement with those presented in Ref. [1] but provide the extended 2D-information. To reveal an advantage of co-solvents as compared to each other, it is necessary to collate their characteristics in detail. Accounting for the above finding on the growth rate saturation and preferring a lower level of dopant to minimize its penetration into SiC crystal, the results of 2D-computations are presented below at 20, 30, 40, and 50 mol.% of co-solvents.

2.2. Si-Cr solution

Fig. 2 illustrates 2D-distributions of temperature together with velocity vectors (on the left) and carbon mass fraction (on the right) in Si-Cr melt-solution at various target temperatures and compositions. Note that the names of regions and the points where the target temperatures are tuned up to keep the drop of 10 K between them are shown in the first picture.

One can see that the flow pattern and the temperature distribution undergo an unnoticeable change in varying the Cr content from 20 to 50 mol.%. A large vortex occupies almost the whole of melt volume with the exception of a small stagnation zone near a central part of the

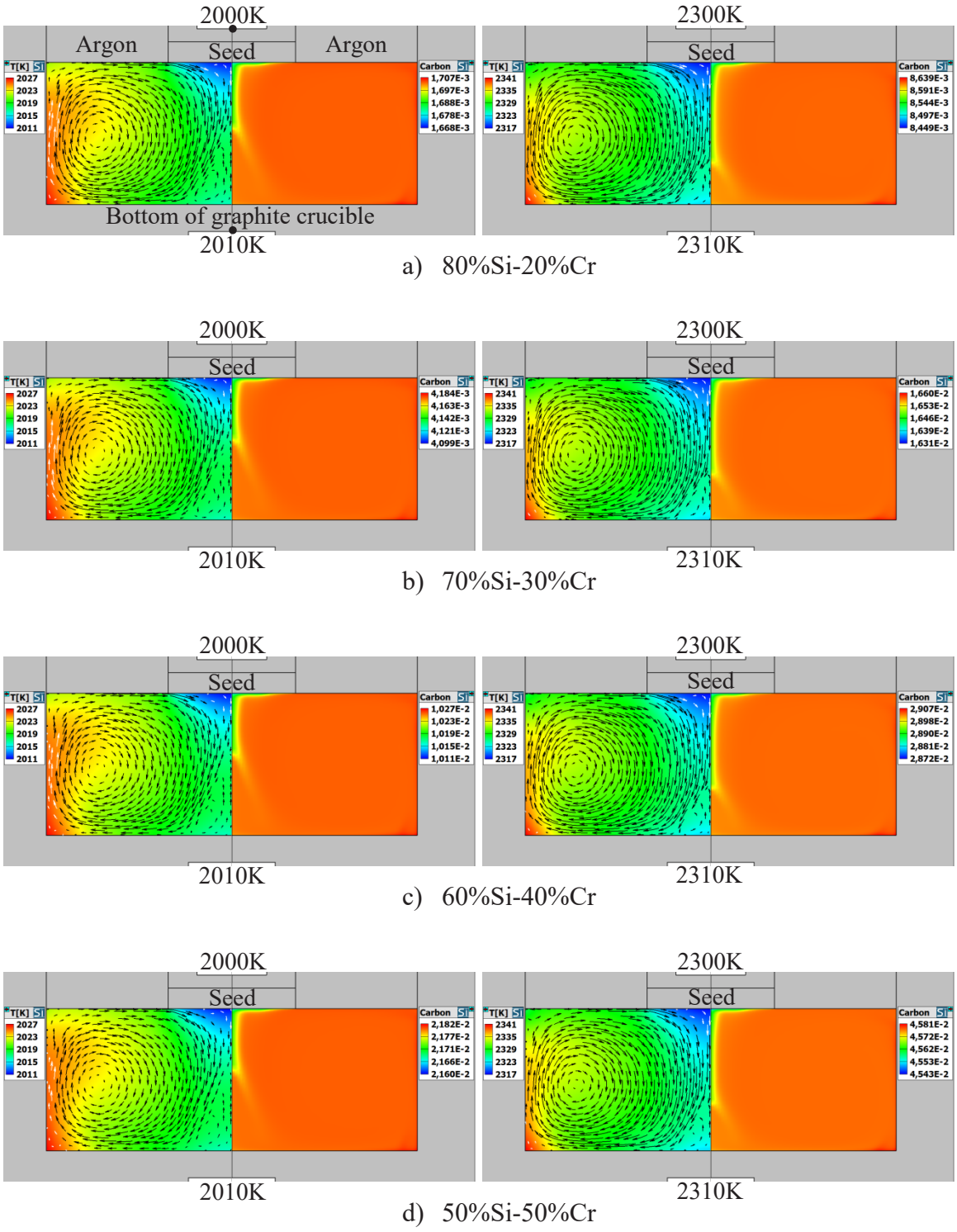

Fig. 2. 2D-distributions of temperature with velocity vectors and carbon mass fraction in Si-Cr solution of various composition. Temperatures shown at top and bottom of growth chamber are kept constant providing 10 K between these points.

crucible bottom. Such flow structure should facilitate an efficient mixing of the binary solution diluted with carbon.

2D-computations predict the melt temperature somewhat higher than the target temperatures at controlled points above the seed and under the bottom. In the case of 2000 and 2010 K (see the left column of pictures) the melt is heated up to 2011–2027 K. If the target temperatures are 2300 and 2310 K (see the right column of pictures), the minimum and maximum temperature is 2317 and 2341 K, respectively. In this connection, the temperature drop in the melt reaches 16 and 24 K in the first and second cases. Thereby, the actual growth temperature can exceed markedly the measured one at controlled point above the seed. On the other hand, a higher growth temperature is accompanied by a less uniform warm-up of the melt.

Unlike the temperature, the mass fraction of carbon turns out to be a sharp function of Cr doping. Its volume-averaged value increases from $1.70\cdot10^{-3}$ to $2.18\cdot10^{-2}$ and from $8.62\cdot10^{-3}$ to $4.57\cdot10^{-2}$ at 2000 and 2300 K above the seed, respectively, when the Cr-percentage varies from 20 to 50%. At the same time, its relative variation in the melt-solution is as low as 2.31% and 1.01% at 2000 K and 2.22% and 0.83% at 2300 K for 20% Cr and 50% Cr, respectively. Such nearly uniform distribution of carbon is an additional support for the efficient mixing due to the small dimension of the crucible. Note that despite less uniform warm-up of the melt at 2300 K, a higher temperature facilitates a slightly lower variation in the carbon mass fraction.

One should pay an additional attention to the fact that a narrow region of relatively reduced mass fraction of carbon stretches from the seed toward the bottom near the melt center. It is somewhat longer at higher temperatures that can be attributed to a higher recirculation velocity and a less deep warm-up of the melt-solution.

Note that the process features considered above influence the crystal surface shape due to non-uniform deposition of the SiC-layers. Fig. 3 demonstrates the radial distribution of SiC growth rate at various Cr-doping and seed top temperatures. As seen from the plots, the growth rate rises with Cr content in varying it from 10 to 50 mol.% at 2000 and 2100 K and from 10 to 40%. at 2200 and 2300 K. At a higher percentage of Cr the growth rate decreases but becomes a smoother function of the seed radius. A near-parabolic convex distribution is predicted beginning with 70% Cr. The maximum growth rate of about 350 μm/h is reached at 40% Cr and at 2300 K of the seed with an essentially non-monotonic radial distribution.

Thus, despite the barely visible dependence of flow and temperature pattern on the melt-solution composition, the Cr-addition can noticeably affect the uniformity of SiC growth rate. As it follows from 2D-computations, the best uniformity is achieved at 70% Cr and higher concentration can cause a foreign inclusion in SiC crystal. It should be noted that the considered dopant gives a minor elevation of the growth rate: 230 μm/h with the near-parabolic distribution is predicted at 2300 K and 70% Cr.

All characteristics listed above are collected in Table 1. Moreover, maximum and averaged values of the growth rate are presented there too. As seen from the data in Table 1, the relative drop of temperature over the melt is constant at Cr-doping varying from 20 to 50% and larger at higher temperature of the process (0.79% at 2000 K and 1.03% at 2300 K). At the same time, the growth rate rises with both temperature and Cr-content.

2.3. Si-La solution

Fig. 4 demonstrates 2D-distributions of temperature together with velocity vectors (on the left) and carbon mass fraction (on the right) in Si-La melt-solution at various target temperatures and compositions.

Unlike Si-Cr solution, a Si/La ratio dependence of the temperature drop over melt becomes noticeable even at the same target temperatures above the seed and under the crucible bottom. The following drops are predicted at temperatures controlled above the seed:

at 2000 K

ΔT = 2028–2010 = 18 K for 20% La,
ΔT = 2028–2009 = 19 K for 30% La,
ΔT = 2029–2009 = 20 K for 40% La,
ΔT = 2030–2008 = 22 K for 50% La;

at 2300 K

ΔT = 2344–2315 = 29 K for 20% La,
ΔT = 2345–2314 = 31 K for 30% La,
ΔT = 2346–2314 = 32 K for 40% La,
ΔT = 2347–2213 = 34 K for 50% La.

One can see that the melt-solution is warming up deeper from the crucible wall to the central with elevating the La-content. Especially, it manifests itself at 2000 K: “hot tongue” penetrates right from side wall up to a middle of the melt. The temperature drop in Si-La solution is significantly higher than that in Si-Cr:

18–22 K for Si-La vs 16 K for Si-Cr at 2000 K;
29–34 K for Si-La vs 24 K for Si-Cr at 2300 K.

This is associated with a difference in such thermophysical properties of Cr and La as thermal conductivity, viscosity, heat capacity, etc. Similarly to the case of Si-Cr, the efficient mixing of Si-La solution is achieved by a large vortex occupying almost the whole of melt volume.

The volume-averaged mass fraction of carbon increases from $5.55\cdot10^{-4}$ to $1.78\cdot10^{-2}$ and from $3.19\cdot10^{-3}$ to $4.48\cdot10^{-2}$ at 2000 K and 2300 K above the seed, respectively, in varying the La-percentage from 20 to 50%. At the same time, its relative variation in the melt-solution

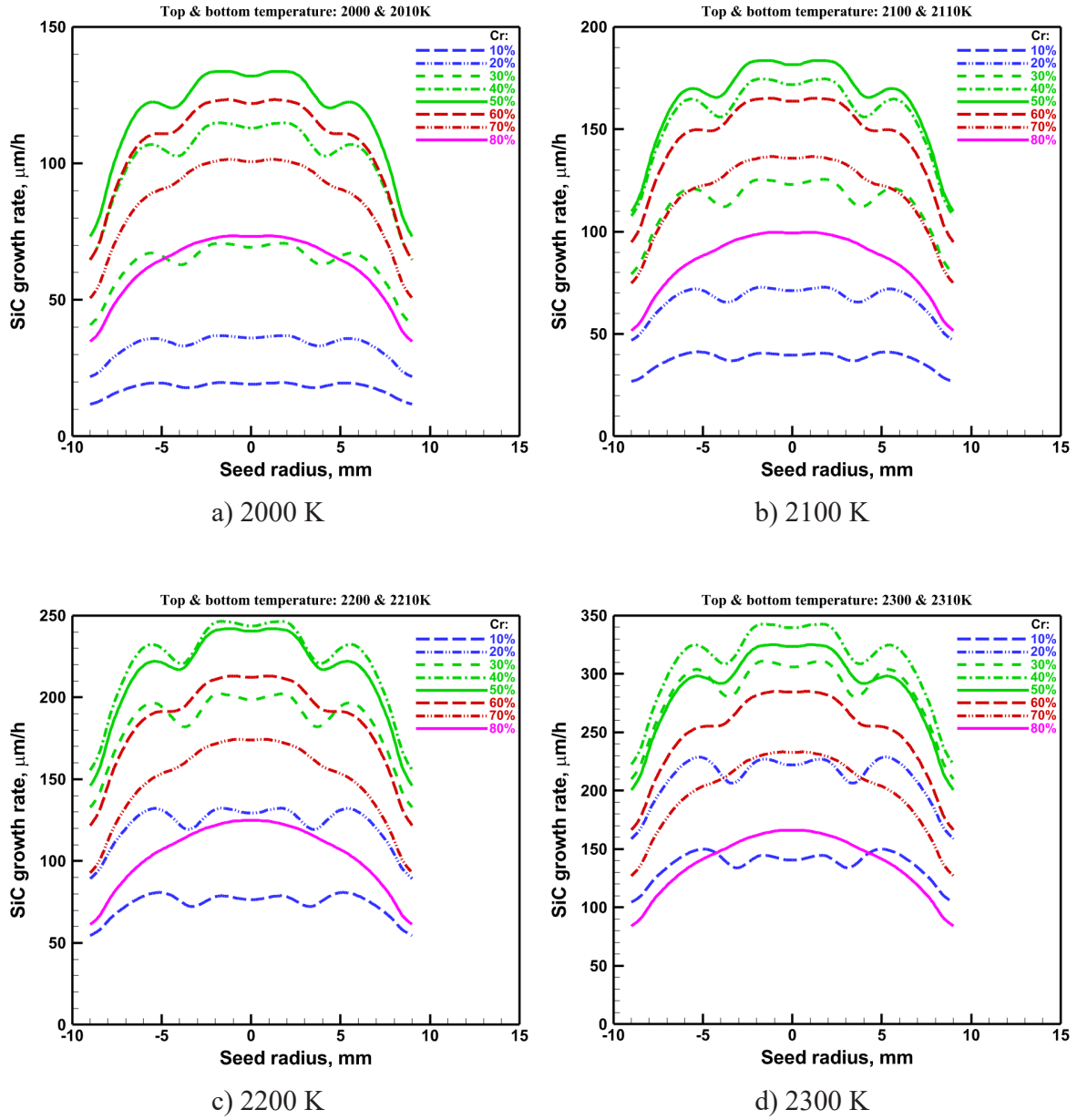

Fig. 3. Radial distribution of SiC growth rate at various Cr-doping and seed top temperatures of a) 2000 K, b) 2100 K, c) 2200 K, and d) 2300 K.

Table 1. Characteristics of Si-Cr solution: drop of temperature, carbon mass fraction over melt, maximum and averaged growth rate.

Si-Cr solution	Temperatures controlled above seed and under bottom	
	2000 and 2010 K	2300 and 2310 K
20% Cr	2011 – 2027 K; 0.79% $1.67 \cdot 10^{-3}$ – $1.71 \cdot 10^{-3}$; 2.29% 37.0 and 31.6 μm/h	2317 – 2341 K; 1.03% $8.45 \cdot 10^{-3}$ – $8.64 \cdot 10^{-3}$; 2.20% 229 and 204 μm/h
30% Cr	2011 – 2027 K; 0.79% $4.10 \cdot 10^{-3}$ – $4.18 \cdot 10^{-3}$; 2.03% 70.7 and 59.6 μm/h	2317 – 2341 K; 1.03% $1.63 \cdot 10^{-2}$ – $1.66 \cdot 10^{-2}$; 1.75% 310 and 273 μm/h
40% Cr	2011 – 2027 K; 0.79% $1.01 \cdot 10^{-2}$ – $1.03 \cdot 10^{-2}$; 1.56% 115 and 95.9 μm/h	2317 – 2341 K; 1.03% $2.87 \cdot 10^{-2}$ – $2.91 \cdot 10^{-2}$; 1.21% 342 and 295 μm/h
50% Cr	2011 – 2027 K; 0.79% $2.16 \cdot 10^{-2}$ – $2.18 \cdot 10^{-2}$; 1.01% 134 and 110 μm/h	2317 – 2341 K; 1.03% $4.54 \cdot 10^{-2}$ – $4.58 \cdot 10^{-2}$; 0.83% 352 and 272 μm/h

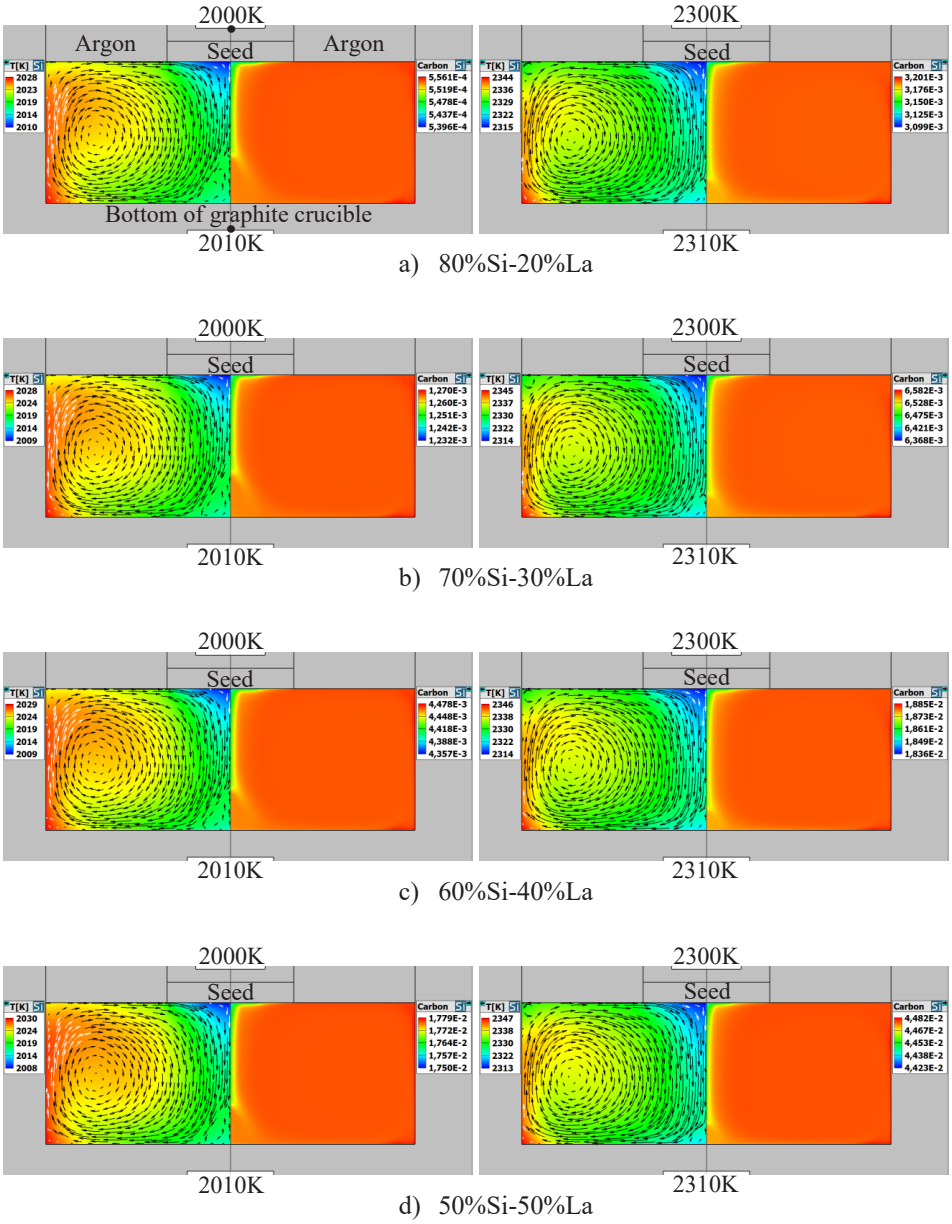

Fig. 4. 2D-distributions of temperature with velocity vectors and carbon mass fraction in Si-La solution of various composition. Temperatures shown at top and bottom of growth chamber are kept constant providing 10K between these points.

is as low as 2.97% and 1.63% at 2000 K and 3.19% and 1.32% at 2300 K for 20% La and for 50% La, respectively. This is markedly higher than in Si-Cr solution.

As opposed to Si-Cr, the observed narrow region of relatively decreased mass fraction of carbon is still more stretched from the seed toward the bottom near the melt center for Si-La solution. Despite the somewhat lower mass fraction of carbon here, SiC growth rate turns out to be higher at La-addition. It can be explained by a strong difference in the carbon distribution and in the mass transport due to convection and diffusion. For instance, the viscosity of La is several times smaller than that of Cr (see Fig. 5 in Ref. [1]) and, therefore, one can expect a larger supply of carbon to the seed.

Fig. 5 shows the radial distribution of SiC growth rate at various La-doping and seed top temperatures. As seen from the plots, the growth rate rises as the La content increases from 10 to 60 mol.% at 2000 and 2100 K and from 10 to 50% at 2200 and 2300 K. At a higher percentage of La the growth rate decreases but becomes a smoother function of the seed radius. A near-parabolic convex distribution is predicted beginning with 70% La. The maximum growth rate of about 1.3 mm/h is reached at 50% La and 2300 K of the seed with an essentially non-monotonic radial distribution.

All characteristics listed above together with maximum and averaged values of the growth rate are collected in Table 2. As it follows from the data in Table 2, the relative drop of temperature over the melt increases from 0.89% to 1.09% at 2000 K and from 1.24% to 1.46% at 2300 K when varying the La-doping from 20 to 50%. At the same time, the growth rate rises with both temperature and La-content.

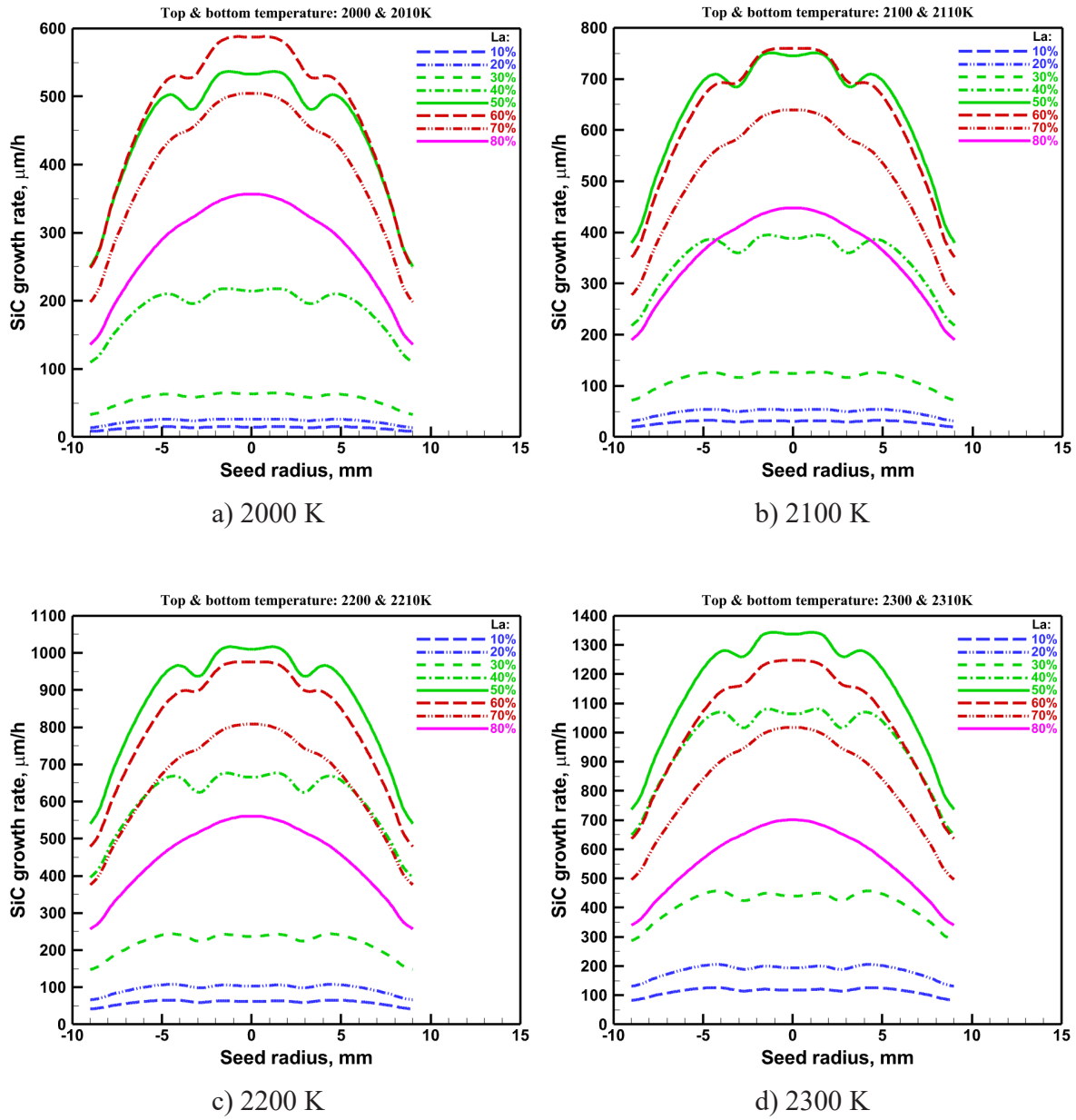

Fig. 5. Radial distribution of SiC growth rate at various La-doping and seed top temperatures of a) 2000 K, b) 2100 K, c) 2200 K, and d) 2300 K.

Table 2. Characteristics of Si-La solution: drop of temperature, carbon mass fraction over melt, maximum and averaged growth rate.

Si-La solution	Temperatures controlled above seed and under bottom	
	2000 and 2010 K	2300 and 2310 K
20% La	2010 – 2028 K; 0.89% $5.39 \cdot 10^{-4}$ – $5.56 \cdot 10^{-4}$; 2.97% 26.6 and 21.9 μm/h	2315 – 2344 K; 1.24% $3.10 \cdot 10^{-3}$ – $3.20 \cdot 10^{-3}$; 3.19% 205 and 176 μm/h
30% La	2009 – 2028 K; 0.94% $1.23 \cdot 10^{-3}$ – $1.27 \cdot 10^{-3}$; 3.00% 64.7 and 52.6 μm/h	2314 – 2345 K; 1.33% $6.37 \cdot 10^{-3}$ – $6.58 \cdot 10^{-3}$; 3.26% 457 and 391 μm/h
40% La	2009 – 2029 K; 0.99% $4.36 \cdot 10^{-3}$ – $4.48 \cdot 10^{-3}$; 2.71% 218 and 175 μm/h	2314 – 2346 K; 1.37% $1.84 \cdot 10^{-2}$ – $1.88 \cdot 10^{-2}$; 2.60% 1081 and 905 μm/h
50% La	2008 – 2030 K; 1.09% $1.75 \cdot 10^{-2}$ – $1.78 \cdot 10^{-2}$; 1.63% 536 and 415 μm/h	2313 – 2347 K; 1.46% $4.42 \cdot 10^{-2}$ – $4.48 \cdot 10^{-2}$; 1.32% 1343 and 1062 μm/h

2.4. Si-Ce solution

Fig. 6 shows 2D-distributions of temperature together with velocity vectors (on the left) and carbon mass fraction (on the right) in Si-Ce melt-solution at various target temperatures and compositions.

As in the case of Si-Cr, the flow pattern and the temperature distribution weakly depend on Ce-content in varying it from 20 to 50 mol.%. A similar large vortex covering almost the whole of melt volume facilitates an efficient mixing of the binary solution diluted with carbon.

Drops of temperature and carbon fraction over the melt, as well as maximum and averaged values of SiC growth rate on the seed are presented in Table 3. As seen from the data, the actual growth temperature can exceed markedly the measured one at controlled point above the seed.

Fig. 7 demonstrates the radial distribution of SiC growth rate at various Ce-doping and seed top temperatures. As it follows from the plots, the growth rate rises with Ce-content in varying it from 10 to 60 mol.% at 2000 and 2100 K and from 10 to 50% at 2200 and 2300 K. At a higher percentage of Ce the growth rate decreases but becomes a smoother function of the seed radius. Its radial distribution is close to convex near-parabolic profile at Ce-doping larger than 70%.

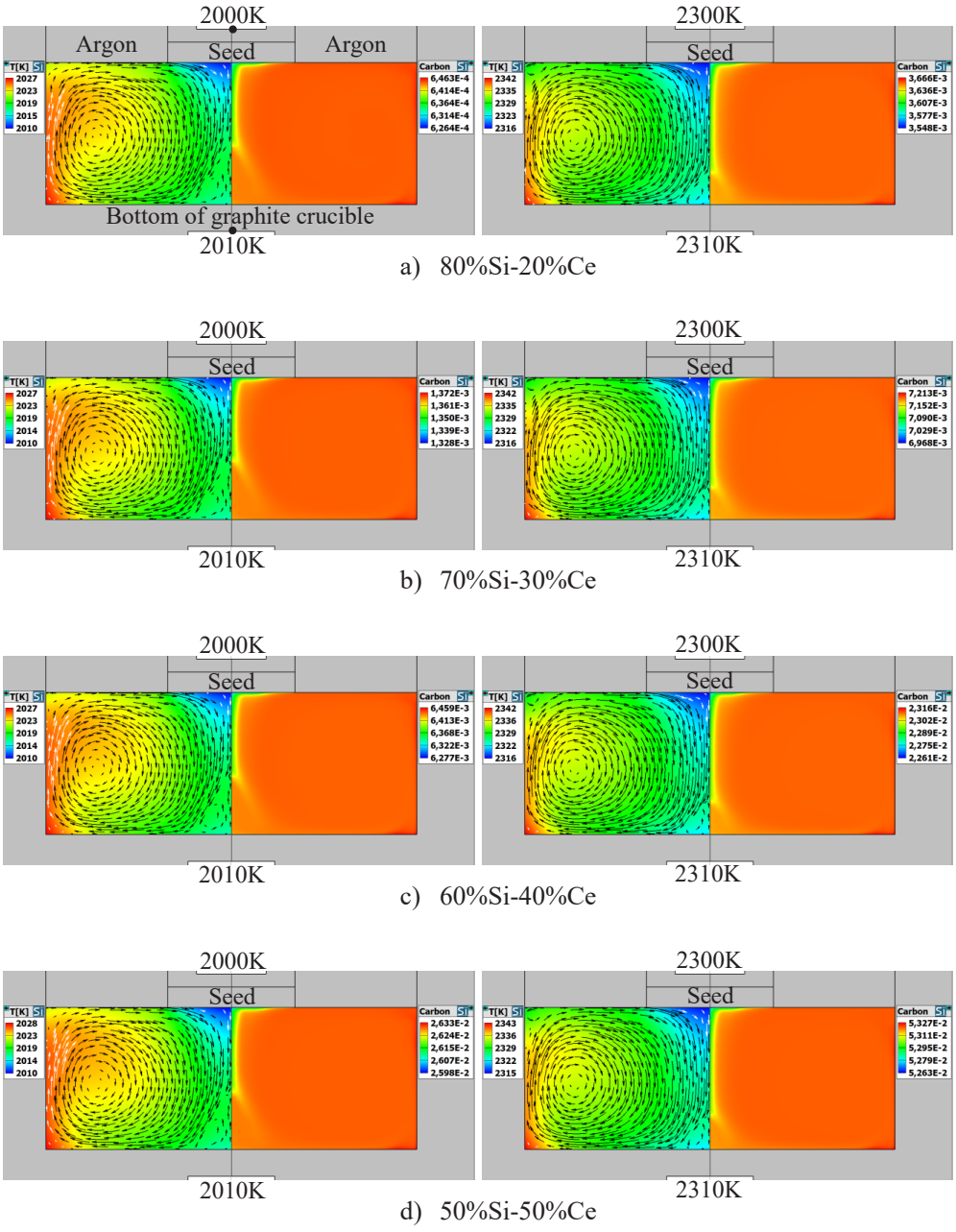

Fig. 6. 2D-distributions of temperature with velocity vectors and carbon mass fraction in Si-Ce solution of various composition. Temperatures shown at top and bottom of growth chamber are kept constant providing 10 K between these points.

Table 3. Characteristics of Si-Ce solution: drop of temperature, carbon mass fraction over melt, maximum and averaged growth rate.

Si-Ce solution	Temperatures controlled above seed and under bottom	
	2000 and 2010 K	2300 and 2310 K
20% Ce	2010 – 2027 K; 0.84% $6.26 \cdot 10^{-4}$ – $6.43 \cdot 10^{-4}$; 3.09% 29.7 and 25.4 μm/h	2316 – 2342 K; 1.11% $3.55 \cdot 10^{-3}$ – $3.67 \cdot 10^{-3}$; 3.23% 218 and 192 μm/h
30% Ce	2010 – 2027 K; 0.84% $1.33 \cdot 10^{-3}$ – $1.37 \cdot 10^{-3}$; 3.22% 68.3 and 58.7 μm/h	2316 – 2342 K; 1.11% $6.97 \cdot 10^{-3}$ – $7.21 \cdot 10^{-3}$; 3.41% 464 and 410 μm/h
40% Ce	2010 – 2027 K; 0.84% $6.28 \cdot 10^{-3}$ – $6.46 \cdot 10^{-3}$; 2.82% 277 and 240 μm/h	2316 – 2342 K; 1.11% $2.26 \cdot 10^{-2}$ – $2.32 \cdot 10^{-2}$; 2.38% 1008 and 889 μm/h
50% Ce	2010 – 2028 K; 0.89% $2.60 \cdot 10^{-2}$ – $2.53 \cdot 10^{-2}$; 1.33% 518 and 432 μm/h	2315 – 2343 K; 1.20% $5.26 \cdot 10^{-2}$ – $5.33 \cdot 10^{-2}$; 1.20% 1124 and 960 μm/h

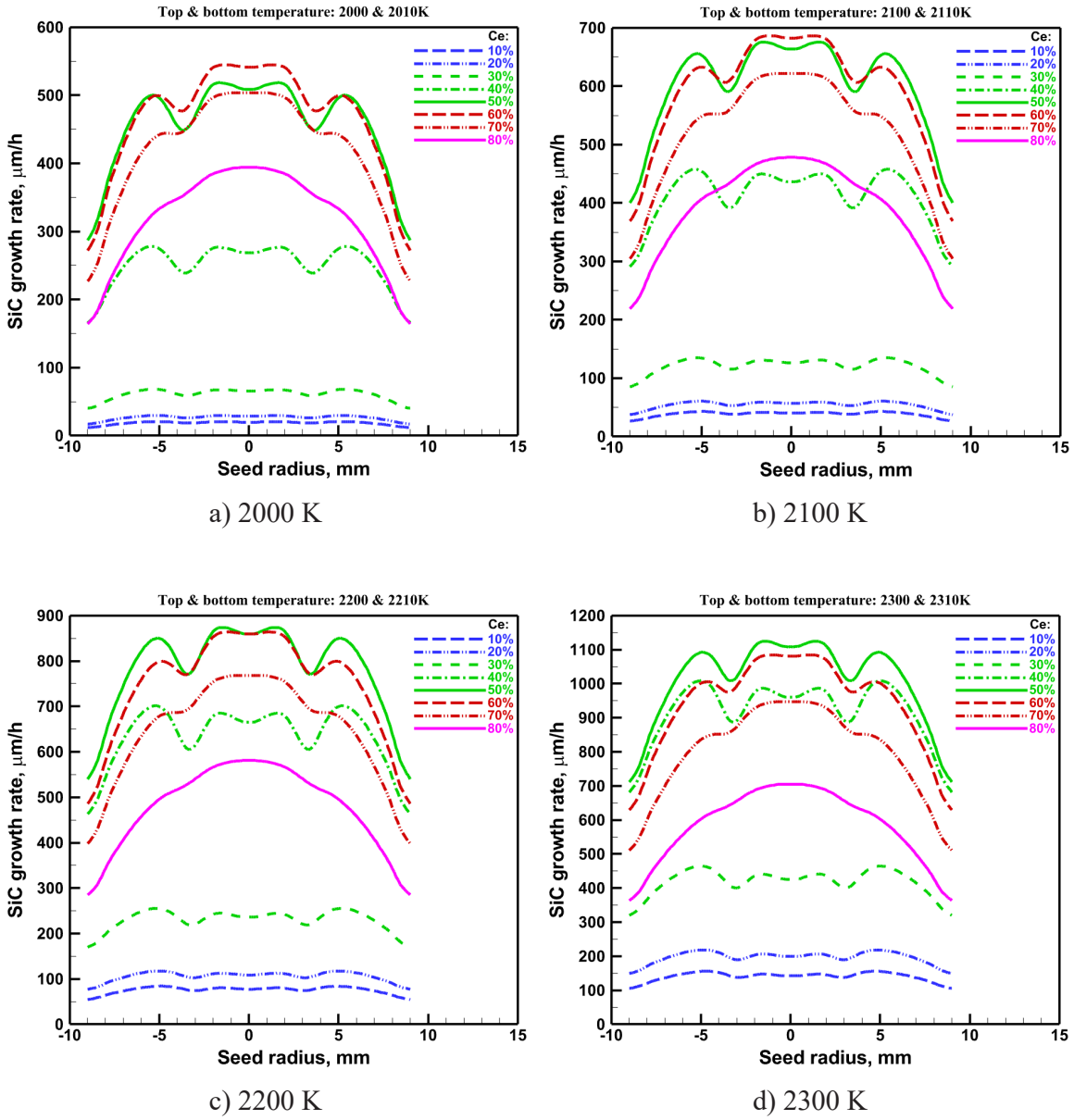

Fig. 7. Radial distribution of SiC growth rate at various Ce-doping and seed top temperatures of a) 2000 K, b) 2100 K, c) 2200 K, and d) 2300 K.

2.5. Si-Pr solution

Fig. 8 illustrates 2D-distributions of temperature together with velocity vectors (on the left) and carbon mass fraction (on the right) in Si-Pr melt-solution at various target temperatures and compositions. Note that they are close to those obtained for Si-Cr and Si-Ce.

One can see that the flow pattern and the temperature distribution undergo similarly an unnoticeable change as Pr-content varies from 20 to 50 mol.%. The details are collected in Table 4. As seen from the data, the relative drop of temperature over the melt increases from 0.84% to 0.89% at 2000 K and from 1.11% to 1.16% at 2300 K as Pr-doping ranges from 20 to 50%.

Fig. 9 demonstrates the radial distribution of SiC growth rate at various Pr-doping and seed top temperatures. As seen from the plots, the growth rate rises with Pr-content in varying it from 10% to 60 mol.% at 2000 and 2100 K and from 10 to 50% at 2200 and 2300 K. A higher percentage of Pr results in a smoother but smaller growth rate. Its convex near-parabolic distribution is predicted beginning with 80% Pr.

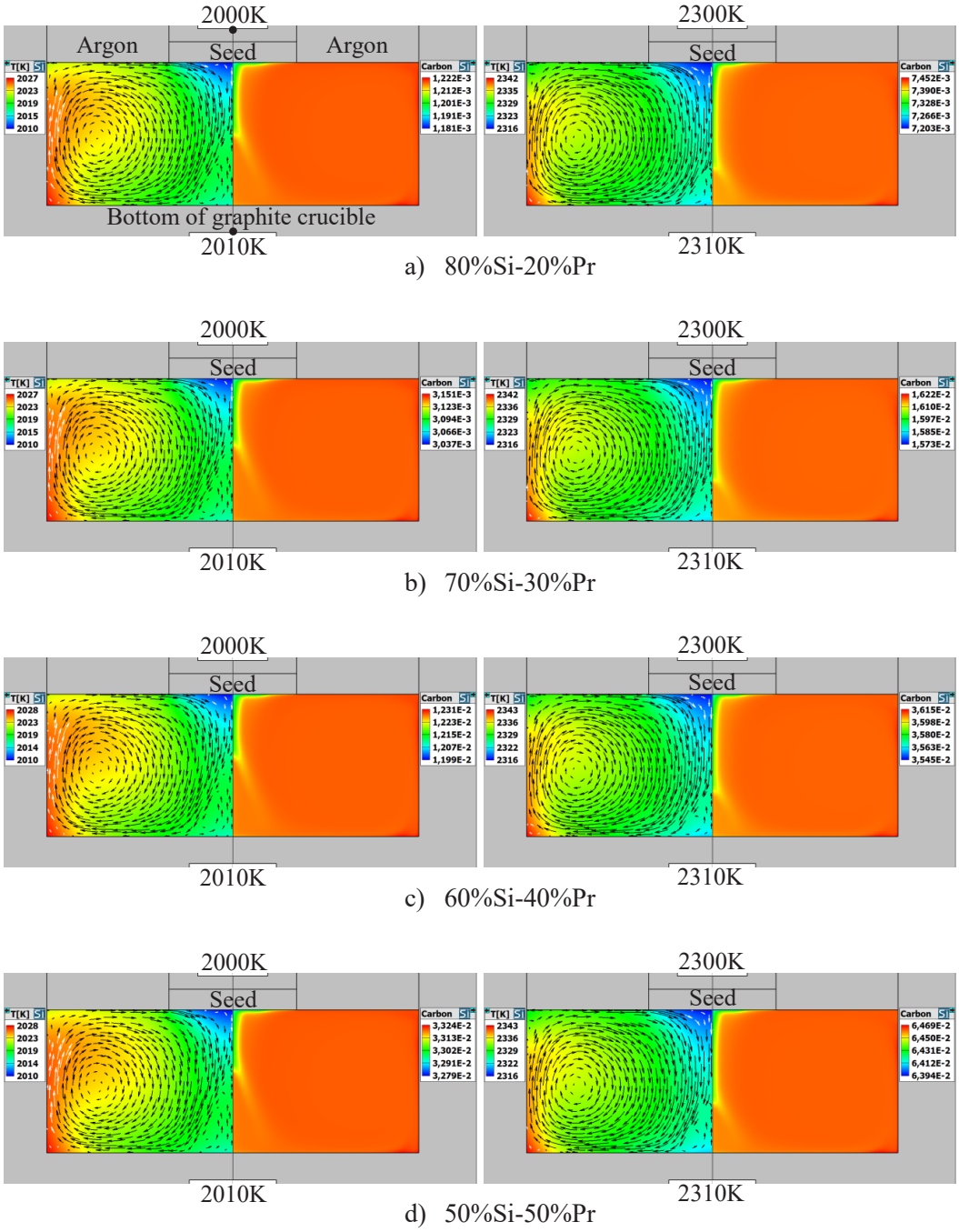

Fig. 8. 2D-distributions of temperature with velocity vectors and carbon mass fraction in Si-Pr solution of various composition. Temperatures shown at top and bottom of growth chamber are kept constant providing 10 K between these points.

Table 4. Characteristics of Si-Pr solution: drop of temperature, carbon mass fraction over melt, maximum and averaged growth rate.

Si-Pr solution	Temperatures controlled above seed and under bottom	
	2000 and 2010 K	2300 and 2310 K
20% Pr	2010 – 2027 K; 0.84% $1.81 \cdot 10^{-3}$ – $1.22 \cdot 10^{-3}$; 3.36% 62.9 and 54.1 μm/h	2316 – 2342 K; 1.11% $7.20 \cdot 10^{-3}$ – $7.45 \cdot 10^{-3}$; 3.52% 218 and 192 μm/h
30% Pr	2010 – 2027 K; 0.84% $3.04 \cdot 10^{-3}$ – $3.15 \cdot 10^{-3}$; 3.63% 176 and 152 μm/h	2316 – 2342 K; 1.11% $1.57 \cdot 10^{-2}$ – $1.62 \cdot 10^{-2}$; 3.03% 950 and 840 μm/h
40% Pr	2010 – 2028 K; 0.89% $1.20 \cdot 10^{-2}$ – $1.23 \cdot 10^{-2}$; 2.60% 494 and 428 μm/h	2316 – 2343 K; 1.16% $3.54 \cdot 10^{-2}$ – $3.61 \cdot 10^{-2}$; 1.94% 1280 and 1132 μm/h
50% Pr	2010 – 2028 K; 0.89% $3.28 \cdot 10^{-2}$ – $3.32 \cdot 10^{-2}$; 1.35% 638 and 542 μm/h	2316 – 2343 K; 1.16% $6.39 \cdot 10^{-2}$ – $6.47 \cdot 10^{-2}$; 1.16% 1330 and 1147 μm/h

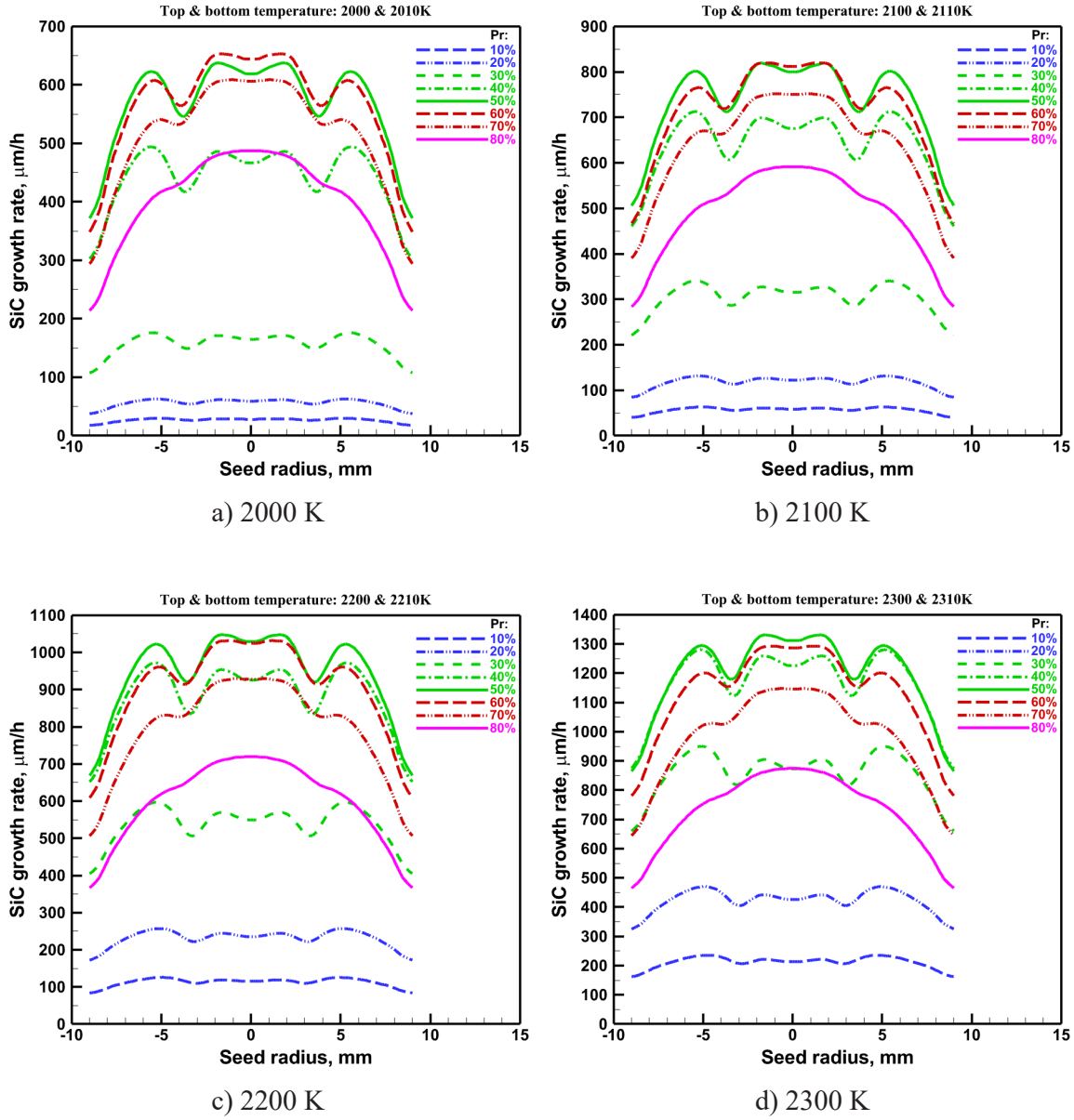

a) 2000 K b) 2100 K

c) 2200 K d) 2300 K

Fig. 9. Radial distribution of SiC growth rate at various Pr-doping and seed top temperatures of a) 2000 K, b) 2100 K, c) 2200 K, and d) 2300 K.

2.6. Si-Nd solution

Fig. 10 illustrates 2D-distributions of temperature together with velocity vectors (on the left) and carbon mass fraction (on the right) in Si-Nd melt-solution at various target temperatures and compositions. Note that they are similar to those obtained for Si-Cr, Si-Ce and Si-Pr.

All features of the case considered are collected in Table 5.

Fig. 11 demonstrates the radial distribution of SiC growth rate at various Nd-doping and seed top temperatures. As seen from the plots, the growth rate rises as Nd content increases from 10 to 60 mol.% with an essentially non-monotonic radial dependence. A further addition of the dopant lowers the growth rate while its radial distribution is smoothed and becomes convex beginning with 80% Nd that can cause a crucial level of foreign inclusion in SiC crystal.

2.7. Si-Y solution

Fig. 12 illustrates 2D-distributions of temperature together with velocity vectors (on the left) and carbon mass fraction (on the right) in Si-Y melt-solution at various target temperatures and compositions. Note that they are similar to those obtained for Si-Cr, Si-Ce and Si-Pr. All features are presented in Table 6.

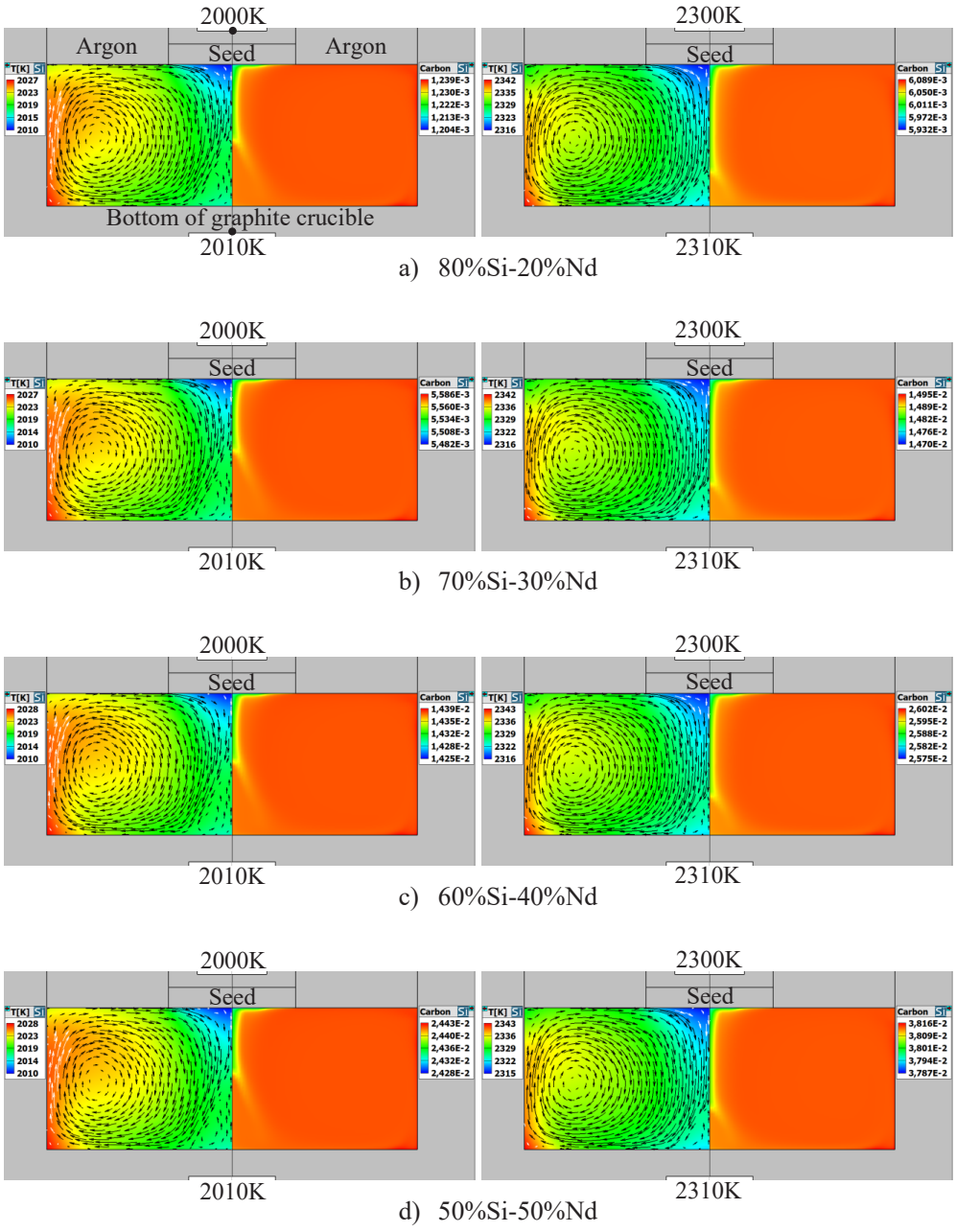

Fig. 10. 2D-distributions of temperature with velocity vectors and carbon mass fraction in Si-Nd solution of various composition. Temperatures shown at top and bottom of growth chamber are kept constant providing 10 K between these points.

Table 5. Characteristics of Si-Nd solution: drop of temperature, carbon mass fraction over melt, maximum and averaged growth rate.

Si-Nd solution	Temperatures controlled above seed and under bottom	
	2000 and 2010 K	2300 and 2310 K
20% Nd	2010 – 2027 K; 0.84% $1.20 \cdot 10^{-3}$ – $1.24 \cdot 10^{-3}$; 2.83% 53.6 and 45.2 μm/h	2316 – 2342 K; 1.11% $5.93 \cdot 10^{-3}$ – $6.09 \cdot 10^{-3}$; 2.58% 309 and 269 μm/h
30% Nd	2010 – 2027 K; 0.84% $5.48 \cdot 10^{-3}$ – $5.59 \cdot 10^{-3}$; 1.86% 170 and 141 μm/h	2316 – 2342 K; 1.11% $1.47 \cdot 10^{-2}$ – $1.49 \cdot 10^{-2}$; 1.67% 492 and 428 μm/h
40% Nd	2010 – 2028 K; 0.89% $1.42 \cdot 10^{-2}$ – $1.44 \cdot 10^{-2}$; 0.97% 235 and 191 μm/h	2316 – 2343 K; 1.16% $2.57 \cdot 10^{-2}$ – $2.60 \cdot 10^{-2}$; 1.04% 558 and 477 μm/h
50% Nd	2010 – 2028 K; 0.89% $2.43 \cdot 10^{-2}$ – $2.44 \cdot 10^{-2}$; 0.61% 254 and 202 μm/h	2315 – 2343 K; 1.20% $3.79 \cdot 10^{-2}$ – $3.82 \cdot 10^{-2}$; 0.76% 593 and 492 μm/h

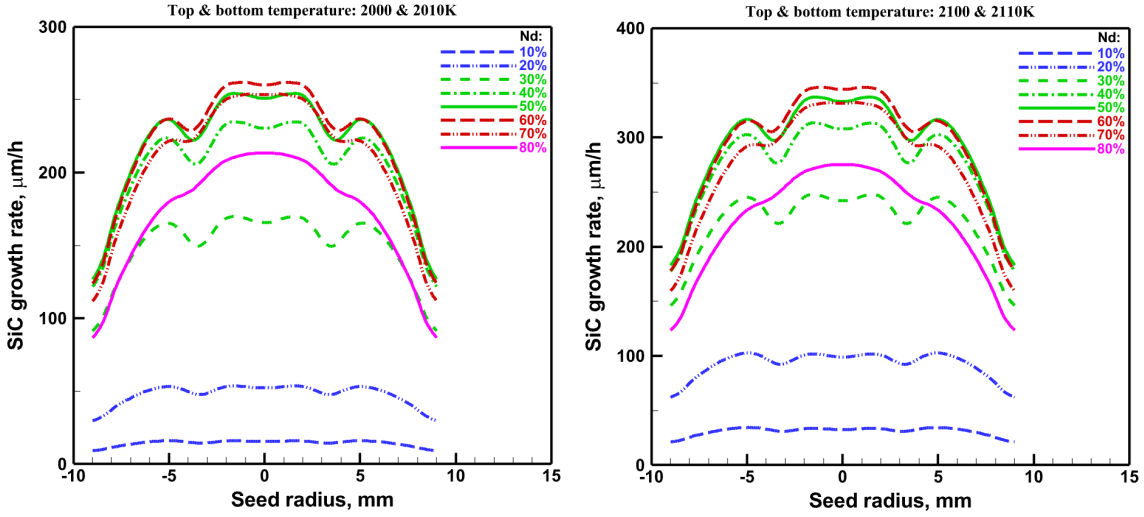

a) 2000 K b) 2100 K

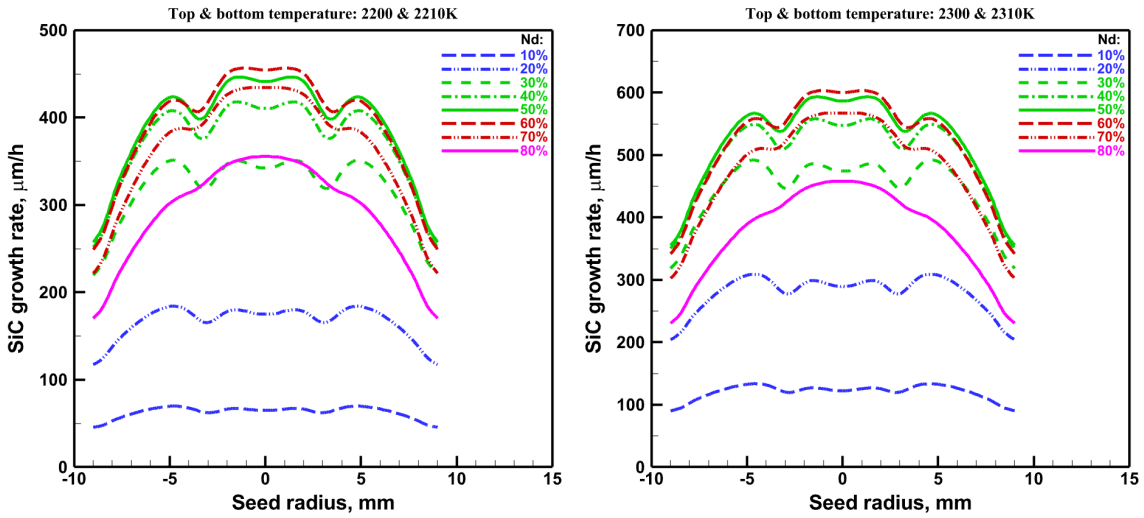

c) 2200 K d) 2300 K

Fig. 11. Radial distribution of SiC growth rate at various Nd-doping and seed top temperatures of a) 2000 K, b) 2100 K, c) 2200 K, and d) 2300 K.

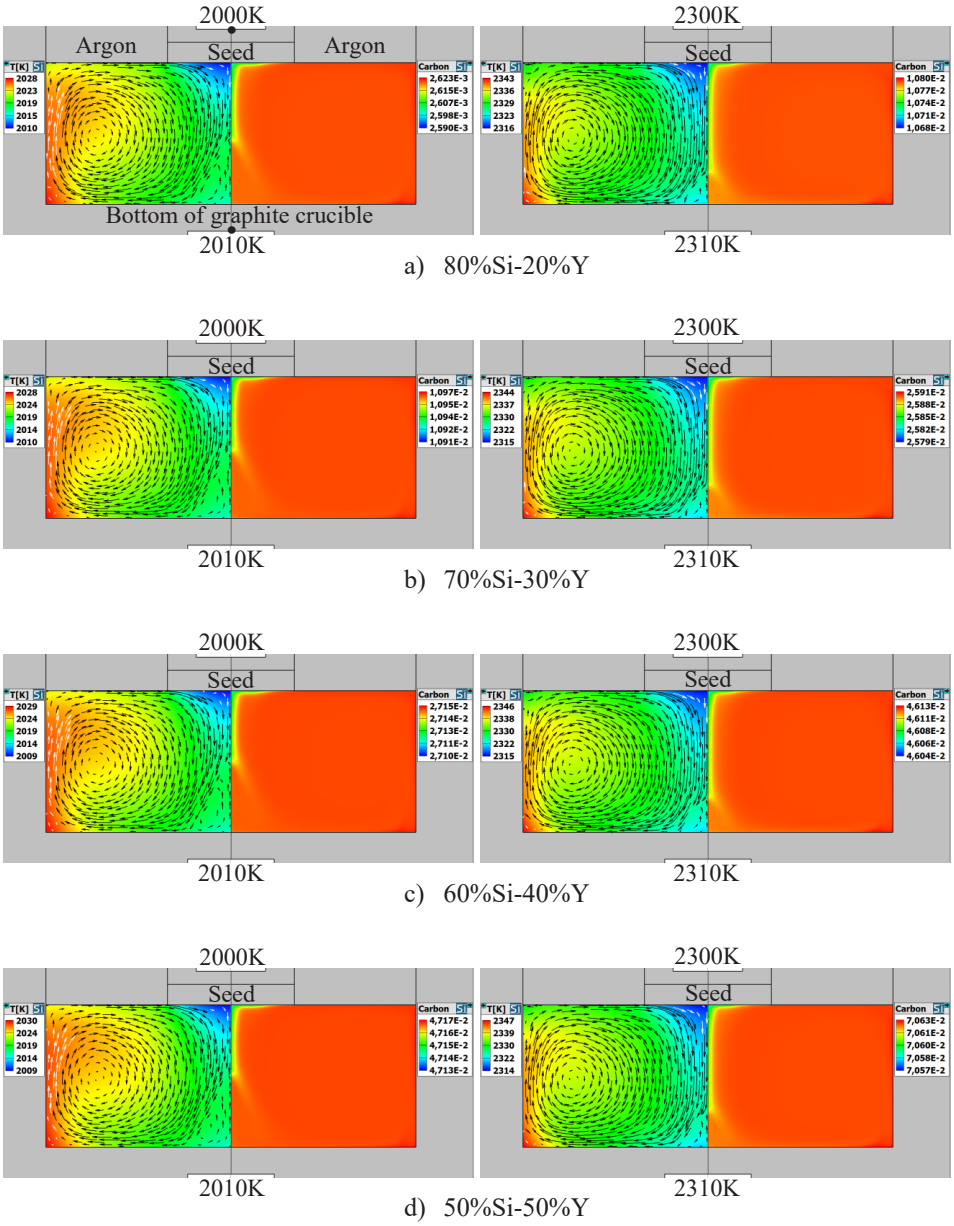

Fig. 12. 2D-distributions of temperature with velocity vectors and carbon mass fraction in Si-Y solution of various composition. Temperatures shown at top and bottom of growth chamber are kept constant providing 10 K between these points.

Table 6. Characteristics of Si-Y solution: drop of temperature, carbon mass fraction over melt, maximum and averaged growth rate.

Si-Y solution	Temperatures controlled above seed and under bottom	
	2000 and 2010 K	2300 and 2310 K
20% Y	2010 – 2028 K; 0.89% $2.59 \cdot 10^{-3}$ – $2.62 \cdot 10^{-3}$; 1.26% 39.5 and 30.1 μm/h	2316 – 2343 K; 1.16% $1.07 \cdot 10^{-2}$ – $1.08 \cdot 10^{-2}$; 1.11% 203 and 163 μm/h
30% Y	2010 – 2028 K; 0.89% $1.09 \cdot 10^{-2}$ – $1.10 \cdot 10^{-2}$; 0.55% 69.1 and 49.8 μm/h	2315 – 2344 K; 1.24% $2.58 \cdot 10^{-2}$ – $2.59 \cdot 10^{-2}$; 0.46% 213 and 160 μm/h
40% Y	2009 – 2029 K; 0.99% $2.72 \cdot 10^{-2}$ – $2.71 \cdot 10^{-2}$; 0.18% 55.5 and 38.6 μm/h	2315 – 2346 K; 1.33% $4.60 \cdot 10^{-2}$ – $4.61 \cdot 10^{-2}$; 0.19% 159 and 115 μm/h
50% Y	2009 – 2030 K; 1.04% $4.71 \cdot 10^{-2}$ – $4.72 \cdot 10^{-2}$; 0.085% 35.3 and 24.2 μm/h	2314 – 2347 K; 1.41% $7.057 \cdot 10^{-2}$ – $7.063 \cdot 10^{-2}$; 0.085% 107 and 75.9 μm/h

Fig. 13 demonstrates the radial distribution of SiC growth rate at various Y-doping and seed top temperatures. As seen from the plots, the growth rate rises with Y content in varying it from 10 to 30 mol.%. At a higher percentage of Y the growth rate decreases but becomes a smoother function of the seed radius. The maximum growth rate of about 210 μm/h is reached at 30% Y and 2300 K of the seed.

Emphasize that Y-addition can noticeably affect the radial dependence of SiC growth rate and, hence, the surface shape of grown crystal. As it follows from the 2D-computations, its convex near-parabolic profile is achieved already at 30% Y that makes Y more preferable compared to other additives due to a low doping and, thereby, a low contamination of the crystal despite a moderate growth rate.

2.8. Si-Me (Me = Fe, Co, Ni, Al, Sc) solutions

2D-distributions of temperature together with velocity vectors and carbon mass fraction in Si-Me (Me = Fe, Co, Ni, Al, Sc) solutions are similar to each other but can differ only in their values. Therefore, all patterns and characteristics related to them are collected in Appendix including the radial dependences of the growth rate. Note that the found trends remain the same with the exception of Si-Al solution. The growth rate increases monotonically with

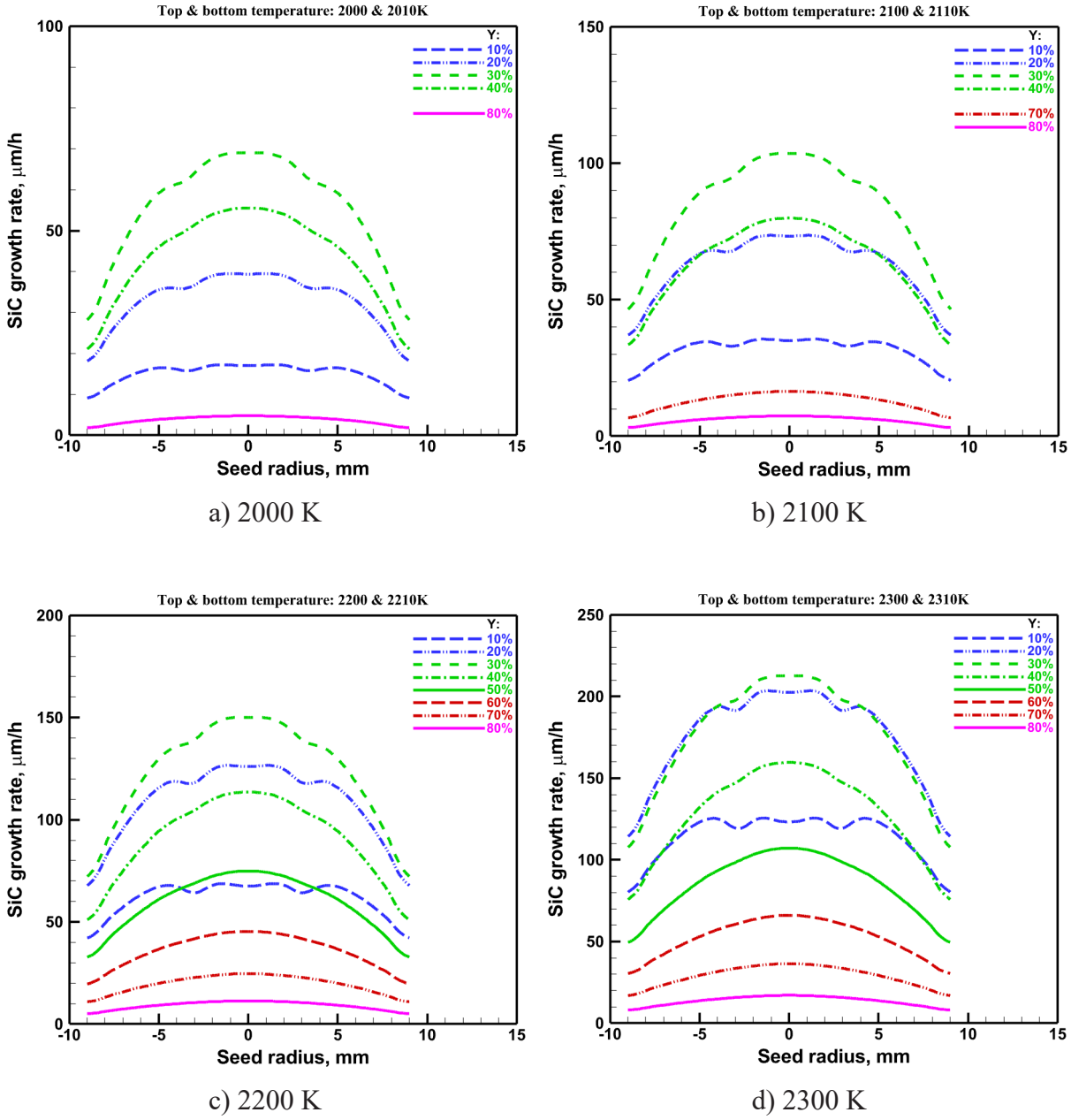

Fig. 13. Radial distribution of SiC growth rate at various Y-doping and seed top temperatures of a) 2000 K, b) 2100 K, c) 2200 K, and d) 2300 K.

Al content varying from 10 to 80 mol.% and no convex near-parabolic distribution is predicted.

2.9. Preliminary comments

The results presented above for binary solutions show that the SiC growth rate, its radial distribution over seed and, hence, the crystal surface shape are considerably influenced by both an additive and its percentage. All additives with the exception of aluminum give rise to the growth rate elevation at their relatively low content and to its subsequent reduction at higher level of doping. At the same time, the radial profile becomes smoother with dopant content, approximating to a convex smooth function. In this connection, to reveal the effect of several solutions on the radial profile and to collate them to each other numerically, the following cubic parabola (V_p) is introduced:

$$V_p = V_{g,\max} - a \cdot r^3 - b \cdot r^2, \tag{1}$$

where

$$a = \frac{20}{r_0^5}\left[\frac{I}{2\pi} - \frac{r_0^2}{4}\left(V_{g,\max} + V_{g,\min}\right)\right],$$

$$b = \frac{1}{r_0^2}\left(V_{g,\max} - V_{g,\min} - r_0^3 a\right),$$

$$I = 2\pi\int_0^{r_0} V_g r dr. \tag{2}$$

Here, r_0 is the seed radius; V_g, $V_{g,\max}$ and $V_{g,\min}$ are the radial distribution of the growth rate over seed surface obtained from 2D-computations, its maximum and minimum values, respectively. The introduced parabola, V_p, possesses the values of $V_{g,\max}$ at $r = 0$ and $V_{g,\min}$ at $r = r_0$ while the area under it equals the integral I in Eq. (2). To evaluate the relative deviation of V_g from its parabolic approximation V_p, the following parameter is applied:

$$\mathrm{dev}\left(V_p, V_g\right) = \frac{\int_0^{r_0} r\left|V_p - V_g\right| dr}{\int_0^{r_0} r V_g dr} \cdot 100\%. \tag{3}$$

Figs. 14–24 demonstrate the radial profiles of growth rate (solid curves) and their approximation by means of the cubic parabolas (dashed curves) at three typical mole fractions of dopants and at two top temperatures of 2000 and 2300 K. Each pair of profiles is accompanied by the relative deviation in percentage terms (3), $\mathrm{dev}\left(V_p, V_g\right)$. One can see from the plots that a higher doping results in a lower deviation from a convex parabolic distribution. Especially, the trend manifests itself at Y-addition (see Fig. 19). The deviation here does not exceed 2% and becomes less than unity already at small Y-doping. The trend is violated only with Al addition (see Fig. 23). Note that the temperature elevation gives a positive effect too.

The dependence of the relative deviation on the dopant content variation in a wide range is presented in Fig. 25 under four growth conditions. The discontinuity of curves corresponding to Y- and Sc-addition indicates that there is no liquid state of Si-Y and Si-Sc alloys within certain temperature-doping region as seen from Si-Y and Si-Sc phase diagrams discussed in the previous paper [1] in detail. As it follows from the dependences obtained, a smoothest profile of the growth rate is predicted for Si-Y solution (green curve) providing a lowest relative deviation of the growth rate from its parabolic approximation. Si-La (dashed red curve), Si-Cr (solid red curve) and Si-Nd (dashed dot dot red curve) systems demonstrate a good result, particularly, at high dopant percentage. The considered feature of rest binary alloys is much worse and worst at Al-addition.

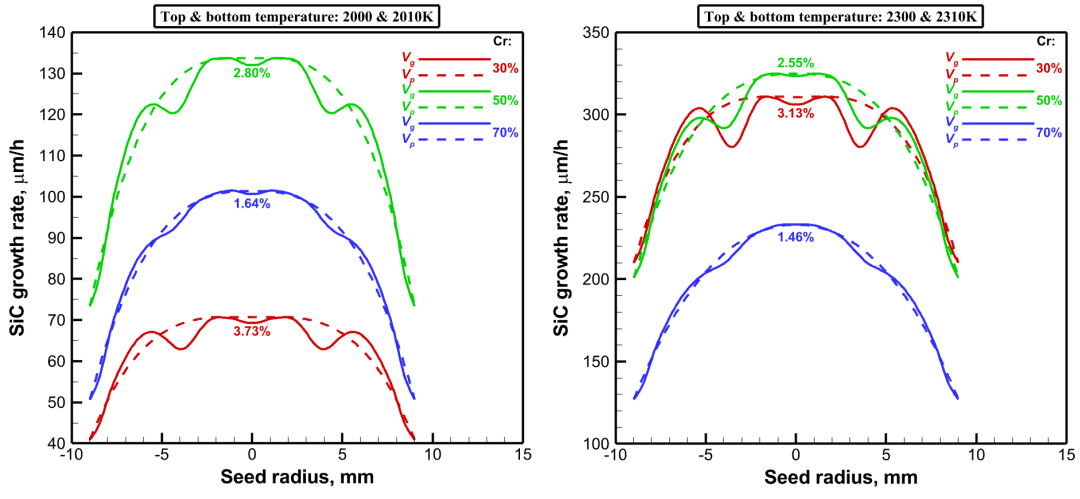

a) b)

Fig. 14. Radial distribution of growth rate at various Cr-content in Si-Cr solution.

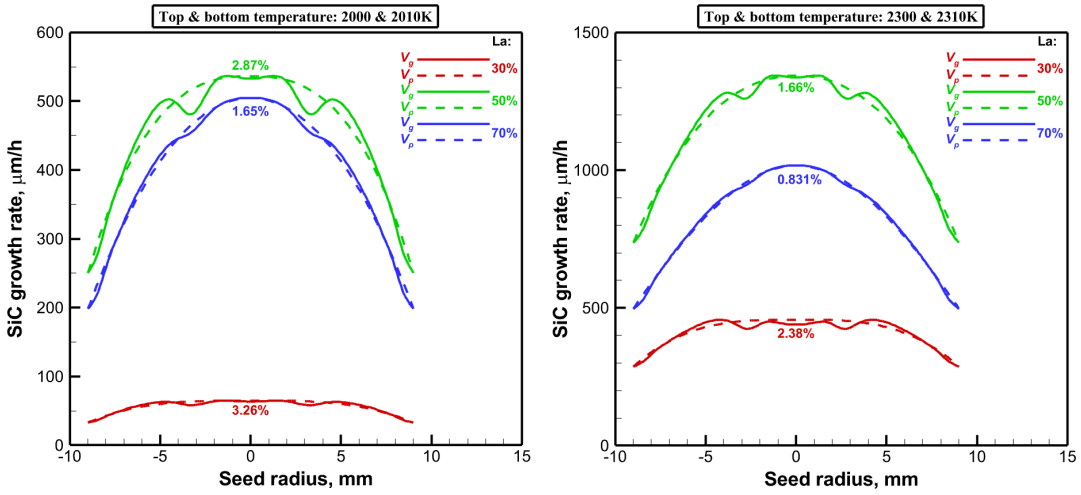

a) b)

Fig. 15. Radial distribution of growth rate at various La-content in Si-La solution.

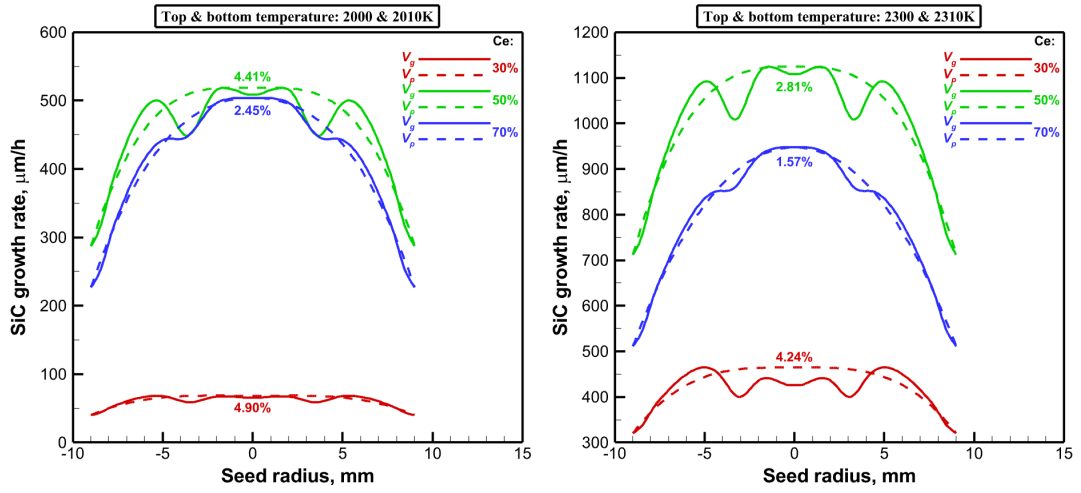

a) b)

Fig. 16. Radial distribution of growth rate at various Ce-content in Si-Ce solution.

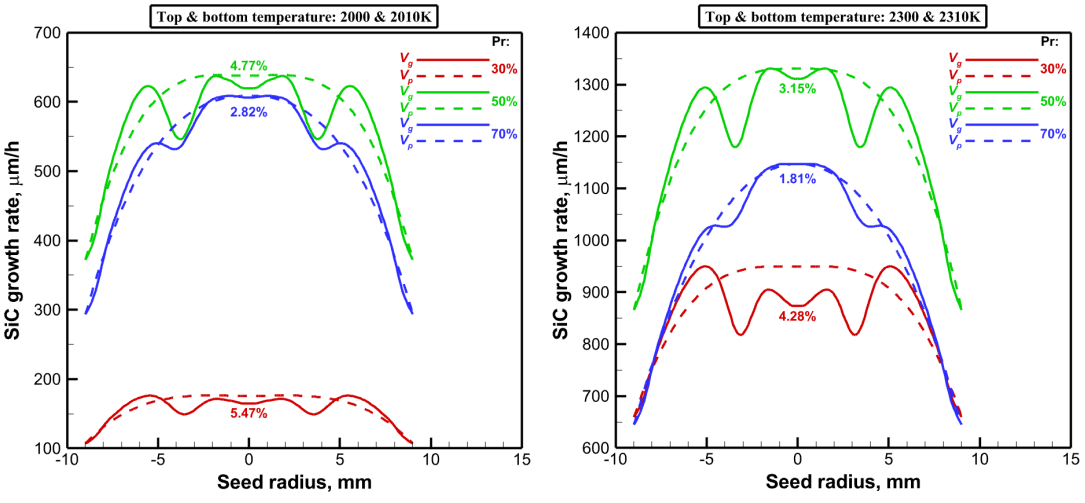

a) b)

Fig. 17. Radial distribution of growth rate at various Pr-content in Si-Pr solution.

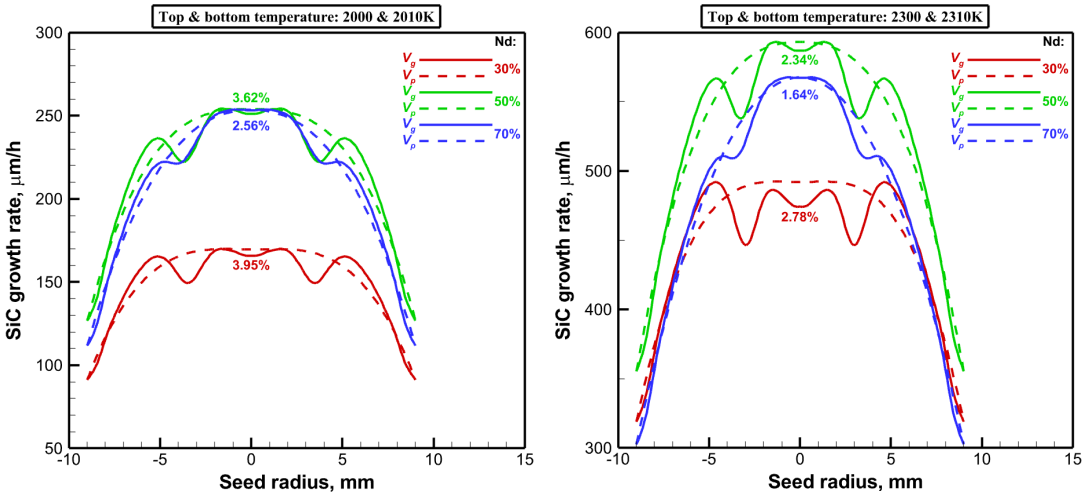

a) b)

Fig. 18. Radial distribution of growth rate at various Nd-content in Si-Nd solution.

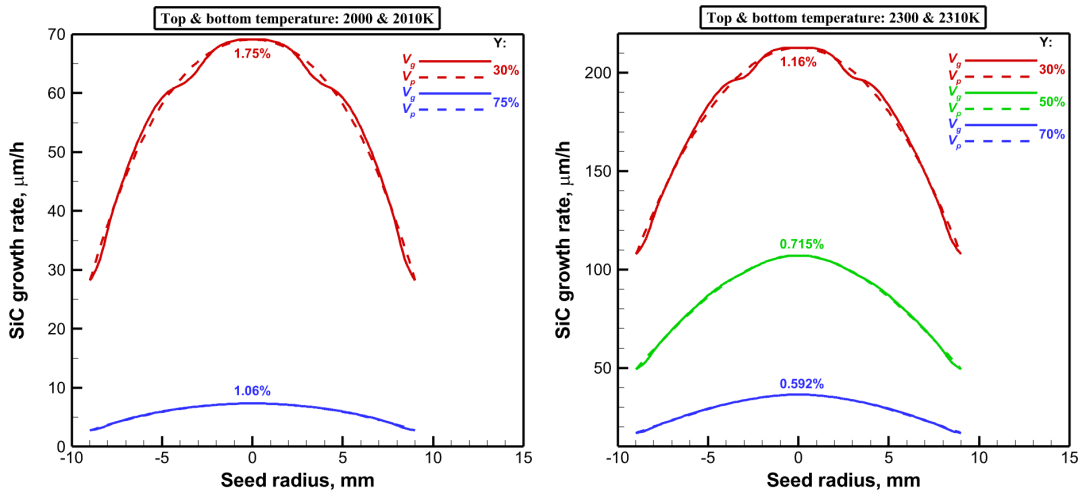

a) b)

Fig. 19. Radial distribution of growth rate at various Y-content in Si-Y solution.

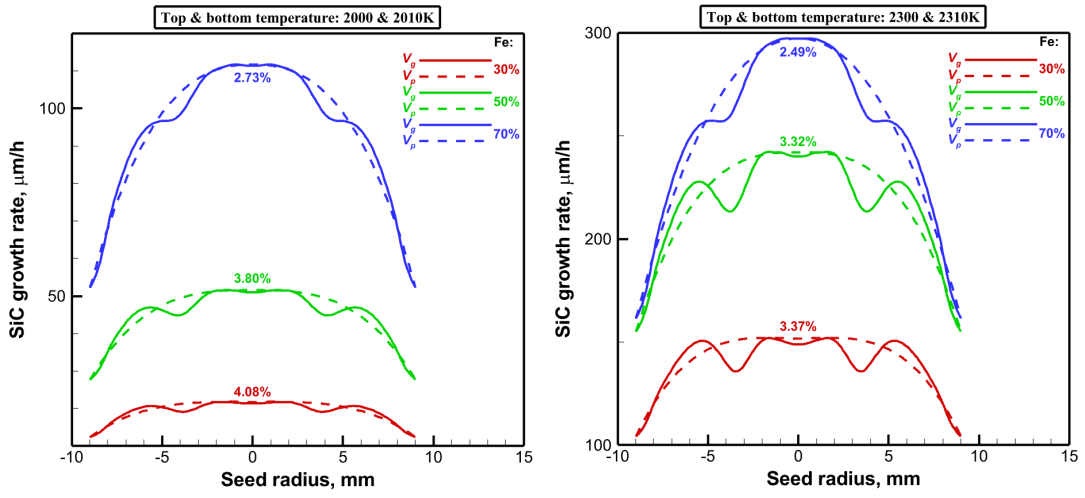

a) b)

Fig. 20. Radial distribution of growth rate at various Fe-content in Si-Fe solution.

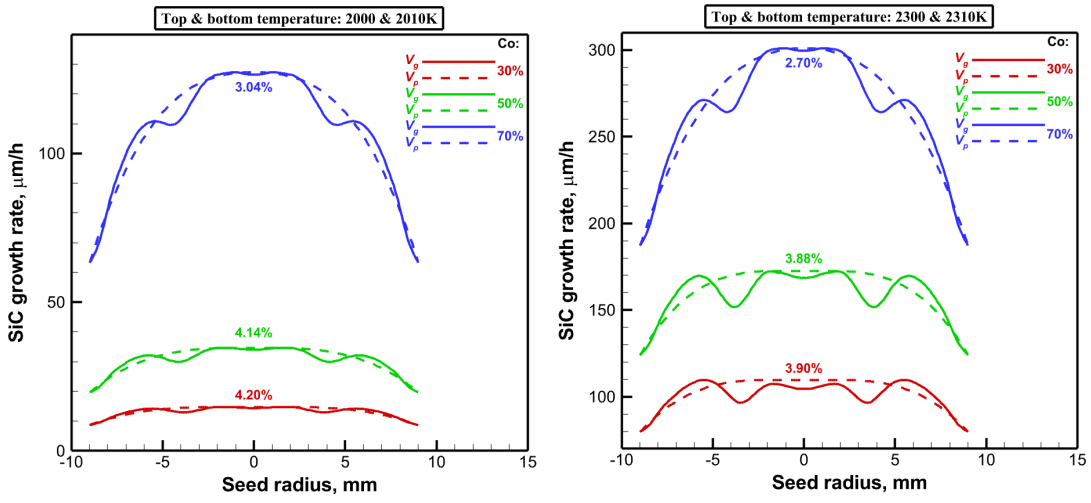

a) b)

Fig. 21. Radial distribution of growth rate at various Co-content in Si-Co solution.

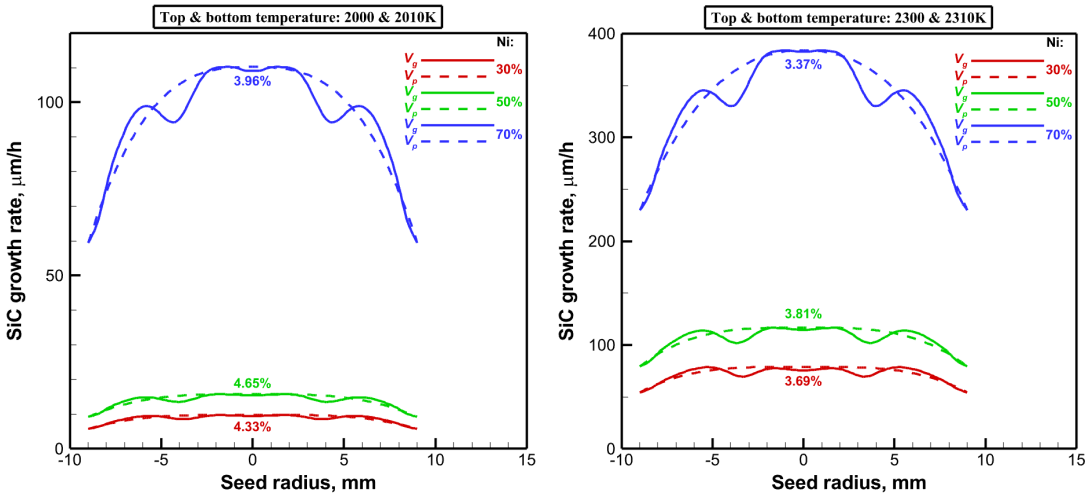

a) b)

Fig. 22. Radial distribution of growth rate at various Ni-content in Si-Ni solution.

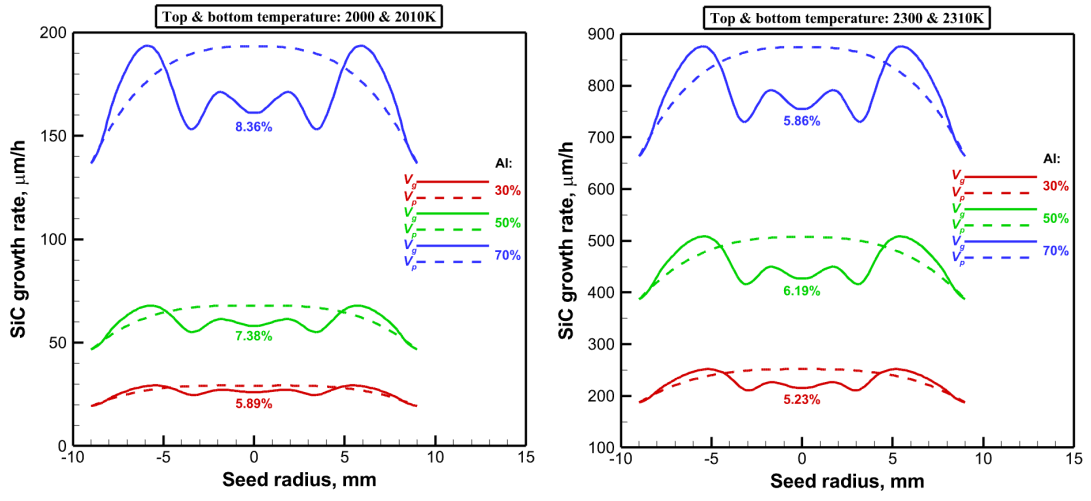

a) b)

Fig. 23. Radial distribution of growth rate at various Al-content in Si-Al solution.

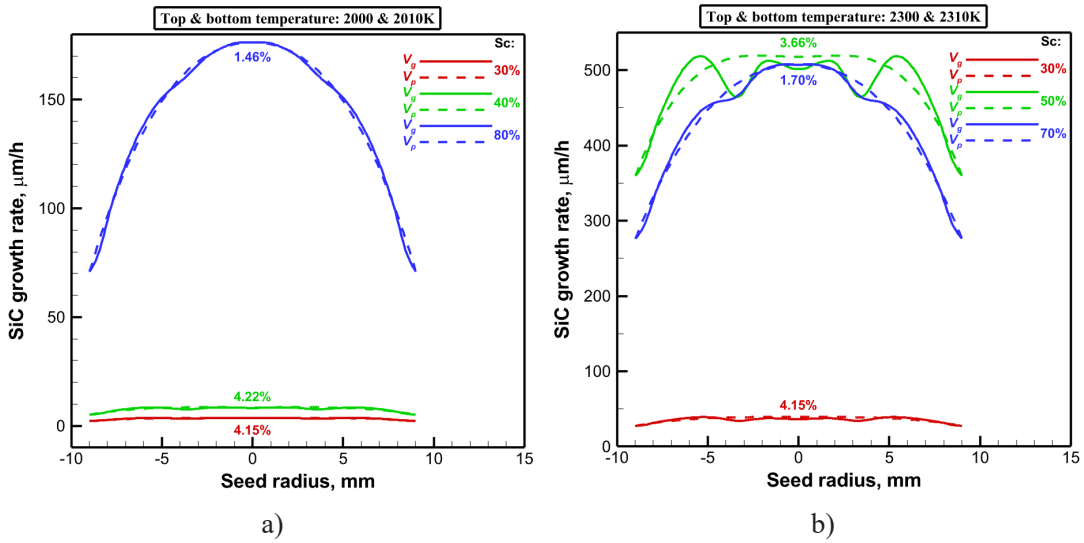

Fig. 24. Radial distribution of growth rate at various Sc-content in Si-Sc solution.

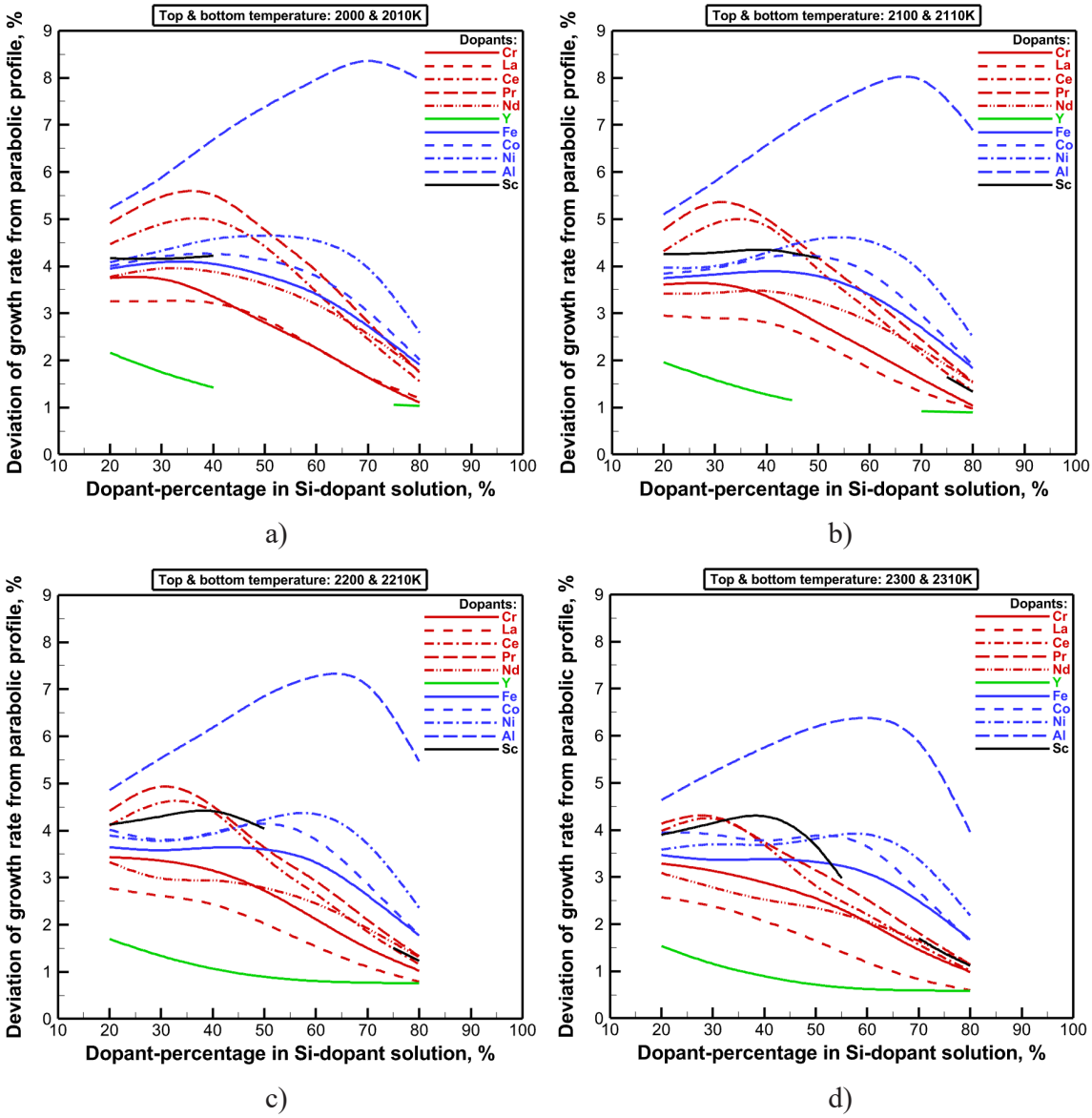

Fig. 25. Relative deviation of growth rate from its parabolic approximation in binary solutions.

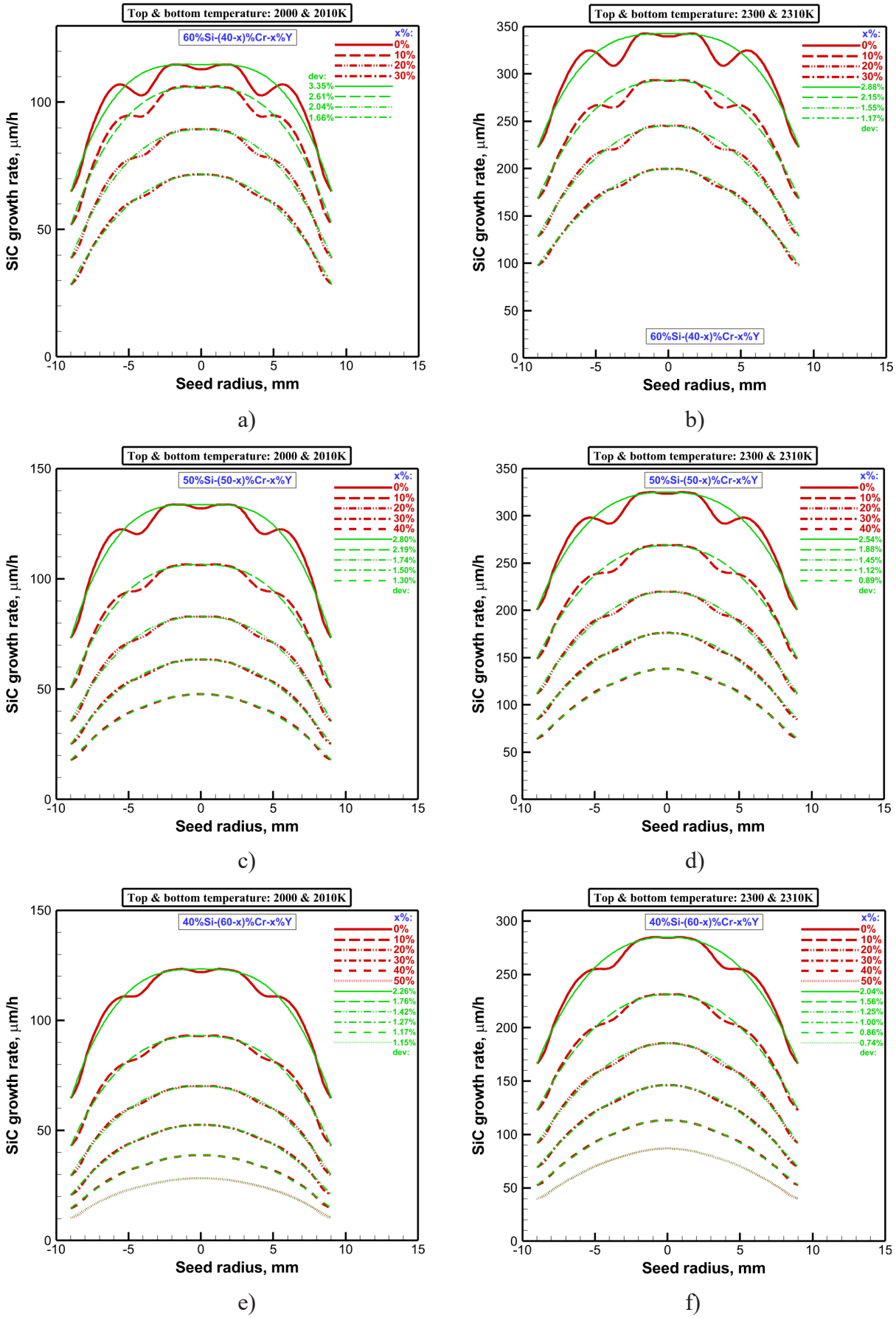

Fig. 26. Radial distribution of growth rate at various Cr/Y ratios in Si-Cr-Y solution.

From the analysis one can conjecture that Y-addition to some binary solution should smooth the surface of SiC growing crystal. With account of a relatively high growth rate and a low deviation of its radial profile from convex parabola, Si-Cr and Si-La systems can be expected as most promising ones in this connection. Therefore, such ternary solutions as Si-Cr-Y and Si-La-Y are investigated below.

3. TERNARY SOLUTIONS: Si-Cr-Y AND Si-La-Y

For simulating the SiC crystal growth from multi-component solutions, it is necessary to know the carbon solubility. To calculate it for ternary solutions within the thermodynamic approach expanded in Ref. [1], Cr-Y and La-Y interaction parameters of excess Gibbs energy should be added to Si-Cr, Si-La, Si-Y, Si-C, Cr-C, La-C, Y-C listed in Table 2 of the previous paper [1]. Their values are collected in Table 7 of the present paper.

Emphasize again that all 2D-computations of SiC crystal growth from solutions above are carried out by CGSim software [18] at the same process parameters and for the same reactor design described in Section 2.1.

3.1. Si-Cr-Y solution

Fig. 26 demonstrates the effect of a partial replacement of chromium by yttrium on the radial distributions of the growth rate at three fixed mole fractions of silicon (60, 50 and 40%) and two typical temperatures over the seed (2000 and 2300 K). Here, the red curves depict the growth rate obtained from 2D-computations while the green ones correspond to their parabolic approximations according to the formulae (1) and (2). The values of relative deviation (dev) calculated from Eq. (3) are shown by green color. As it follows from the results, the crystal surface is smoothed with Y-doping. Support for this comes from the fact that the radial distribution of the actual growth rate tends to a convex parabolic profile that is confirmed by a simultaneous decrease of the relative deviation. In addition to that, the process temperature elevation gives a remarkable smoothing. For instance, 50%Si-(50–*x*)% Cr-*x*%Y solution allows one to provide an acceptable near-parabolic radial distribution of the growth rate at 30% Y (see Figs. 26c and d). Therewith, the maximum values of about 50 μm/h and 150 μm/h are achieved at 2000 and 2300 K, respectively. They are lower than in Si-Cr solution without Y-doping.

Fig. 27 illustrates the relative deviation of the growth rate from its parabolic approximation at varying the Si-Cr-Y composition in a wide range. One can see that the deviation falls down with the gradual Cr-to-Y transition. The growth temperature increase from 2000 to 2300 K enhances the trend.

So, Y-addition to Si-Cr solution in substitution for Cr is predicted to smooth the crystal surface and to reduce the growth rate at the same time. Therefore, one has to search for a compromise between these two opposite trends.

Table 7. Additional binary interaction parameters of excess Gibbs energy description.

$$\Delta G^{ex}_{i-j} = x_i x_j \sum_{k=0}^{N} \left({}^{k}a_{i-j} + {}^{k}b_{i-j} T \right) \left(x_i - x_j \right)^k, \ \mathrm{J \cdot mole^{-1}}$$

i-j	${}^{0}a_{i-j}$; ${}^{0}b_{i-j}$	${}^{1}a_{i-j}$; ${}^{1}b_{i-j}$	Refs.
Cr-Y	3200.0; 0.00	8500.0; 0.00	[20]
La-Y	–350.0; 0.00	0.00; 0.00	[21]

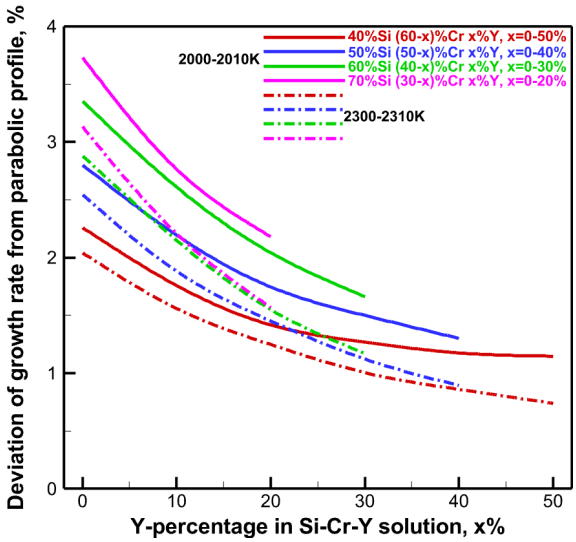

Fig. 27. Relative deviation of growth rate from its parabolic approximation vs Cr/Y ratio in ternary Si-Cr-Y solution.

3.2. Si-La-Y solution

2D-simulations show that the partial replacement of lanthanum by yttrium gives the effect similar to that revealed for Si-Cr-Y solution. Fig. 28 illustrates it at the same process parameters. Y-addition in substitution for La results in both monotonic reduction of the growth rate and smoothing of its radial distribution.

As an example, let us consider 50% Si-(50–*x*)%La-*x*%Y solution again. 20% Y turns out to be sufficient to reach the relative deviation of 1.06% at the top temperature of 2300 K (see Fig. 28d). On the other hand, the growth rate of about 400 μm/h is predicted that is remarkably higher than that in Si-Cr-Y system at the same Cr/Y ratio. In comparison with 2300 K, the relative deviation is only 1.88% at 2000 K (see Fig. 28c), confirming the better smoothing of the crystal surface due to the growth temperature elevation.

The reduction of silicon content to 40 mol.% smooths additionally the growth rate profile and provides the deviation of 0.98% already at 10% Y when the top temperature is 2300 K (see Fig. 28f). At the same time, the rather high

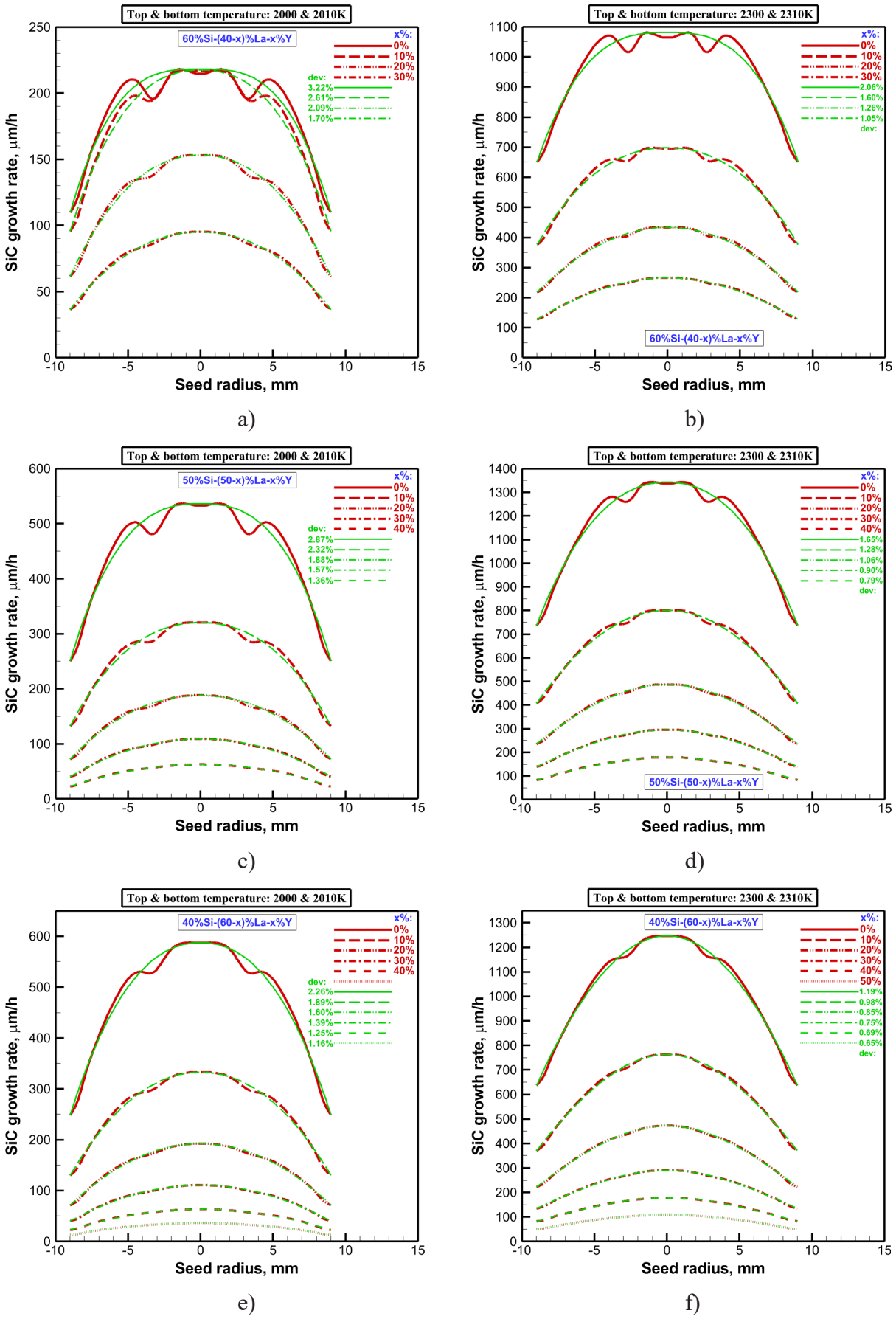

Fig. 28. Radial distribution of growth rate at various La/Y ratios in Si-La-Y solution.

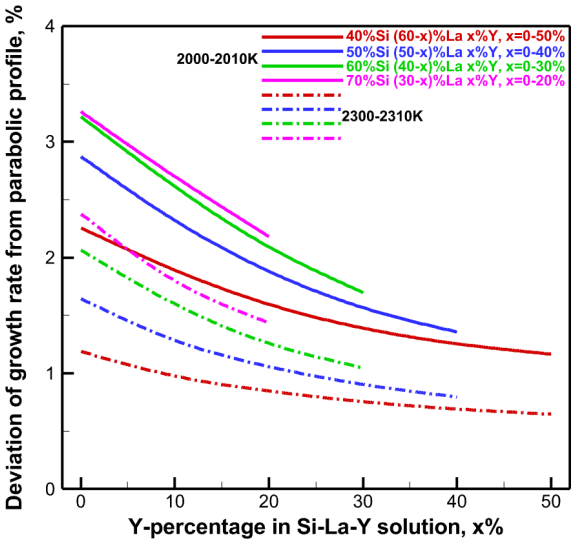

Fig. 29. Relative deviation of growth rate from its parabolic approximation vs La/Y ratio in ternary Si-La-Y solution.

growth rate of about 600–700 μm/h is predicted under these conditions. The further elevation of Y mole fraction to 30% lowers the deviation to 0.75% and the growth rate to 200 μm/h. One can see that a smoother profile corresponding to a smaller deviation goes with a decrease in the growth rate.

Fig. 29 shows the relative deviation of the growth rate from its parabolic approximation as a function of La/Y ratio at fixed mole fraction of silicon. Note that in comparison with Si-Cr-Y system (see Fig. 27), an addition of yttrium instead of lanthanum gives a steeper dependence of the deviation on temperature. For instance, the transition from 2000 to 2300 K decreases the deviation from 2.61% to 2.15% at 60%Si-30%Cr-10%Y solution whereas the fall from 2.61% to 1.60% is predicted at 60%Si-30%La-10%Y solution.

From the results obtained, one can conclude that for achieving the desirable compromise between the high growth rate and its smooth profile at low foreign inclusions in the crystal, Si-La-Y solution turns out to be the best candidate. Nevertheless, such quaternary solution as Si-Cr-La-Y seems to be of interest too.

Note that the dopant penetration into SiC crystal is a problem requiring a special and deep elaboration.

4. SUMMARY

Sequential 2D-computations of SiC TSSG by CGSim software [18] are conducted for investigating the crystal growth rate and its radial distribution at various temperatures and percentages of 11 co-solvents in binary solutions. It is shown that among others the addition of Cr, lanthanides and Y to the molten silicon turns out to be most promising. Moreover, such ternary solutions as Si-Cr-Y and Si-La-Y are found to provide both relatively high growth rate and its minimum deviation from a convex parabolic profile. It should be noted too that a partial replacement of chromium or lanthanum by yttrium lowers the growth rate but smooths essentially its radial profile.

ACKNOWLEDGEMENTS

The author is grateful to the STR administration in the person of R.A. Talalaev and V.V. Kalaev for opportunity to conduct the present research.

APPENDIX

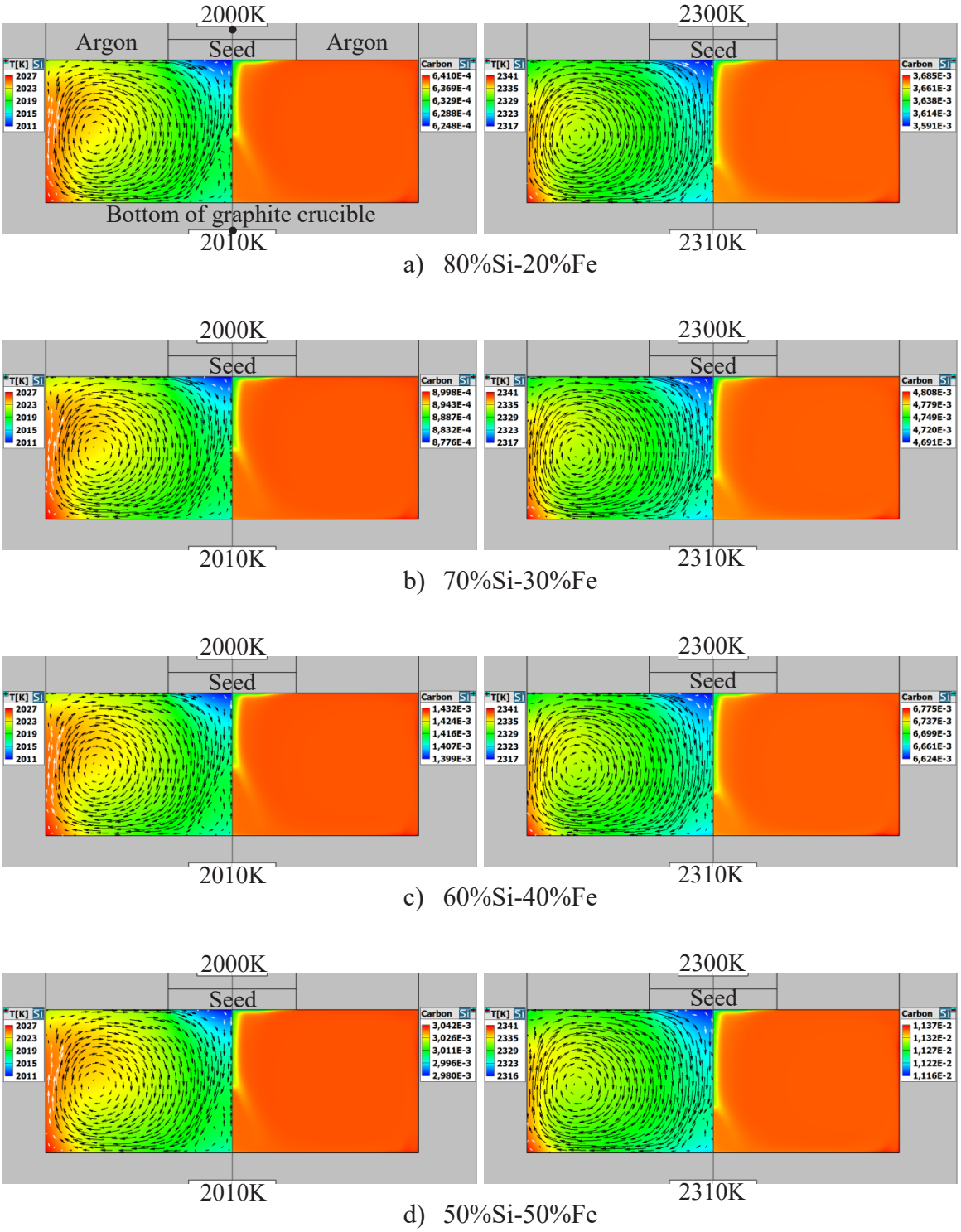

Fig. A1. 2D-distributions of temperature with velocity vectors and carbon mass fraction in Si-Fe solution of various composition. Temperatures shown at top and bottom of growth chamber are kept constant providing 10 K between these points.

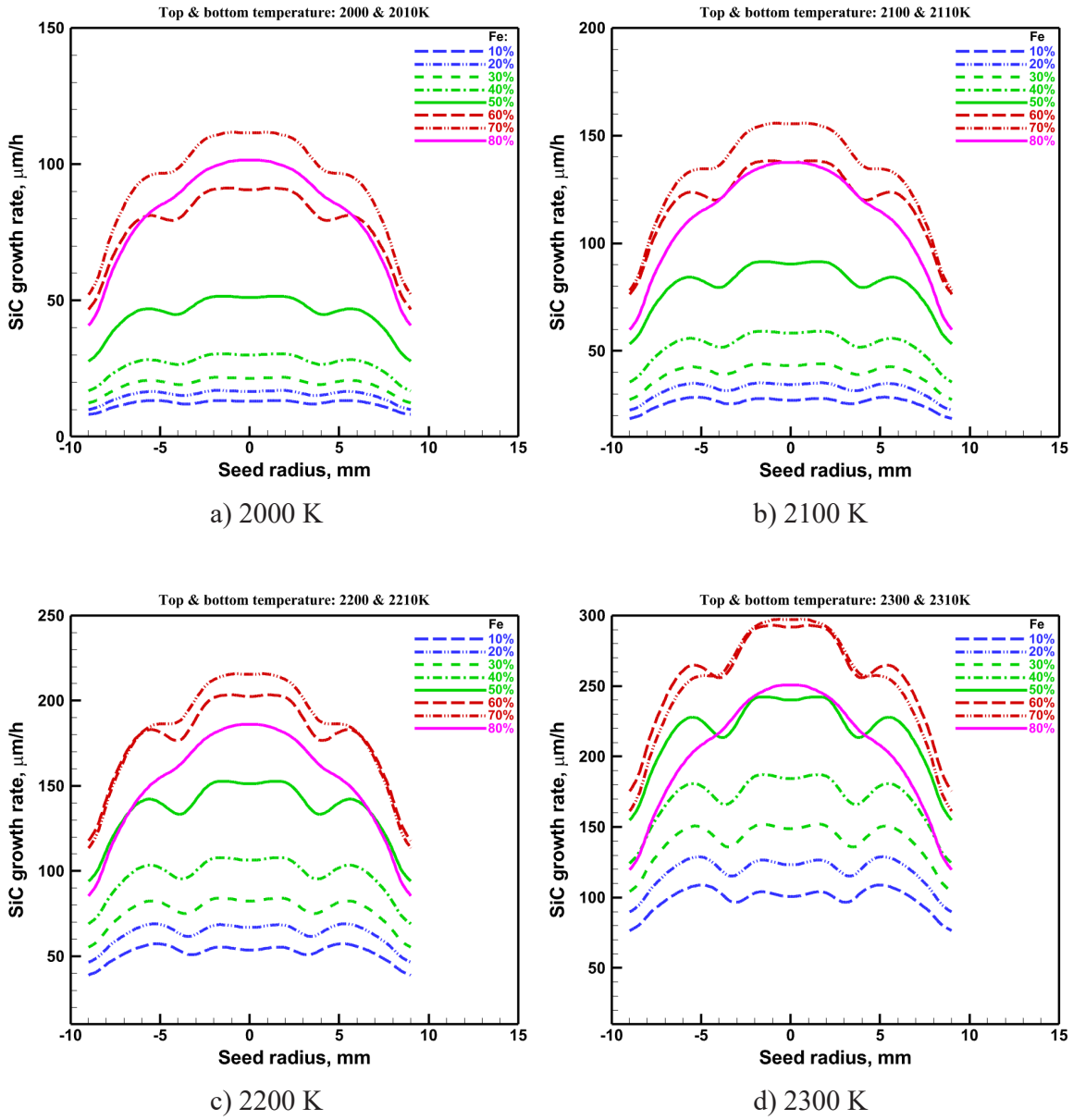

Fig. A2. Radial distribution of SiC growth rate at various Fe-doping and seed top temperatures of a) 2000 K, b) 2100 K, c) 2200 K, and d) 2300 K.

Table A1. Characteristics of Si-Fe solution: drop of temperature, carbon mass fraction over melt, maximum and averaged growth rate.

Si-Fe solution	Temperatures controlled above seed and under bottom	
	2000 and 2010 K	2300 and 2310 K
20% Fe	2011 – 2027 K; 0.79% $6.25 \cdot 10^{-4}$ – $6.41 \cdot 10^{-4}$; 2.53% 17.0 and 14.5 μm/h	2317 – 2341K; 1.03% $3.59 \cdot 10^{-3}$ – $3.68 \cdot 10^{-3}$; 2.56% 129 and 115 μm/h
30% Fe	2011 – 2027K; 0.79% $8.78 \cdot 10^{-4}$ – $9.00 \cdot 10^{-4}$; 2.47% 21.8 and 18.3 μm/h	2317 – 2341K; 1.03% $4.69 \cdot 10^{-3}$ – $4.81 \cdot 10^{-3}$; 2.44% 152 and 135 μm/h
40% Fe	2011 – 2027K; 0.79% $1.40 \cdot 10^{-3}$ – $1.43 \cdot 10^{-3}$; 2.31% 30.4 and 25.1 μm/h	2317 – 2341K; 1.03% $6.62 \cdot 10^{-3}$ – $6.77 \cdot 10^{-3}$; 2.23% 187 and 163 μm/h
50% Fe	2011 – 2027K; 0.79% $2.98 \cdot 10^{-3}$ – $3.04 \cdot 10^{-3}$; 2.04% 51.5 and 42.1 μm/h	2316 – 2341K; 1.07% $1.12 \cdot 10^{-3}$ – $1.14 \cdot 10^{-3}$; 1.85% 242 and 206 μm/h

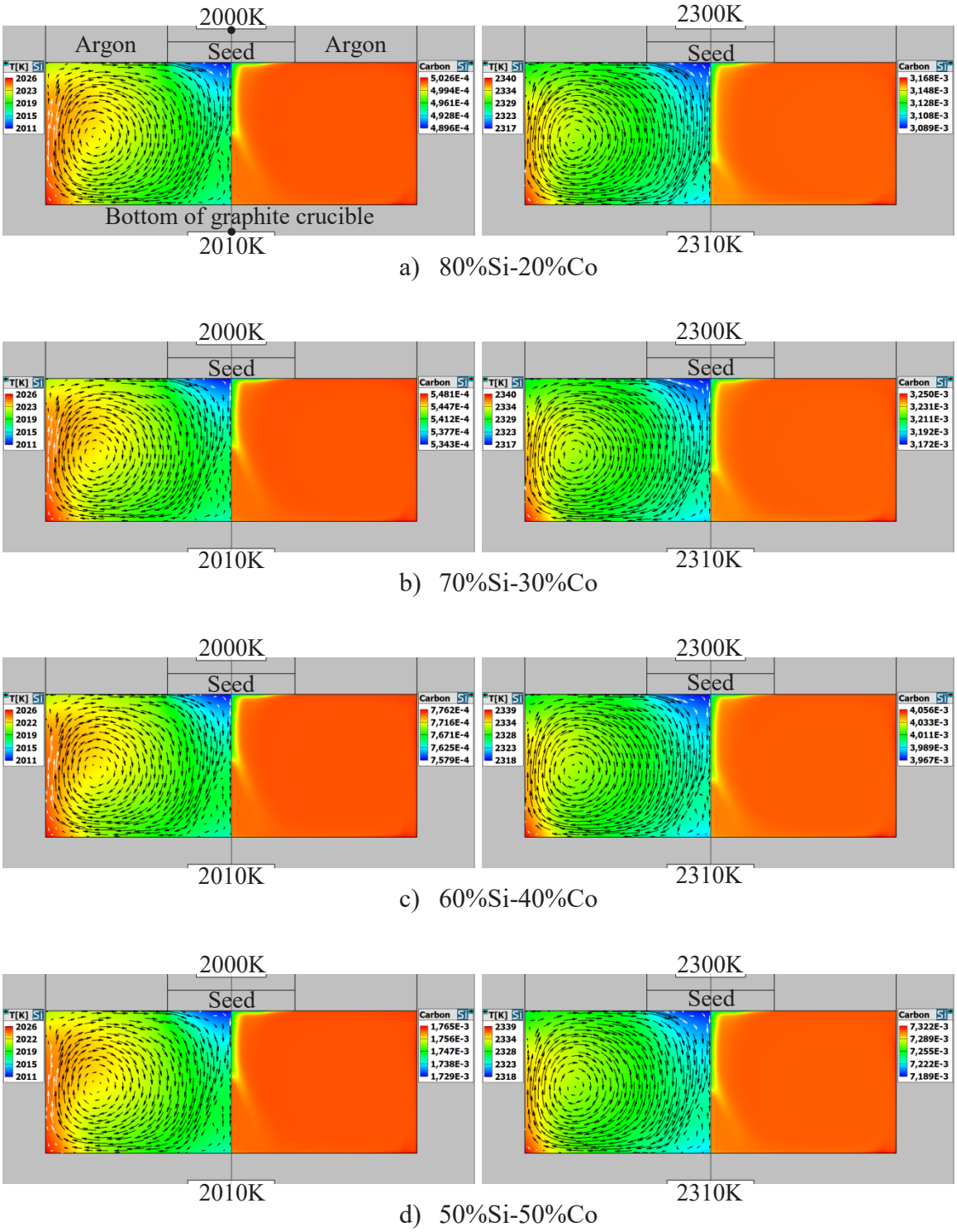

Fig. A3. 2D-distributions of temperature with velocity vectors and carbon mass fraction in Si-Co solution of various composition. Temperatures shown at top and bottom of growth chamber are kept constant providing 10 K between these points.

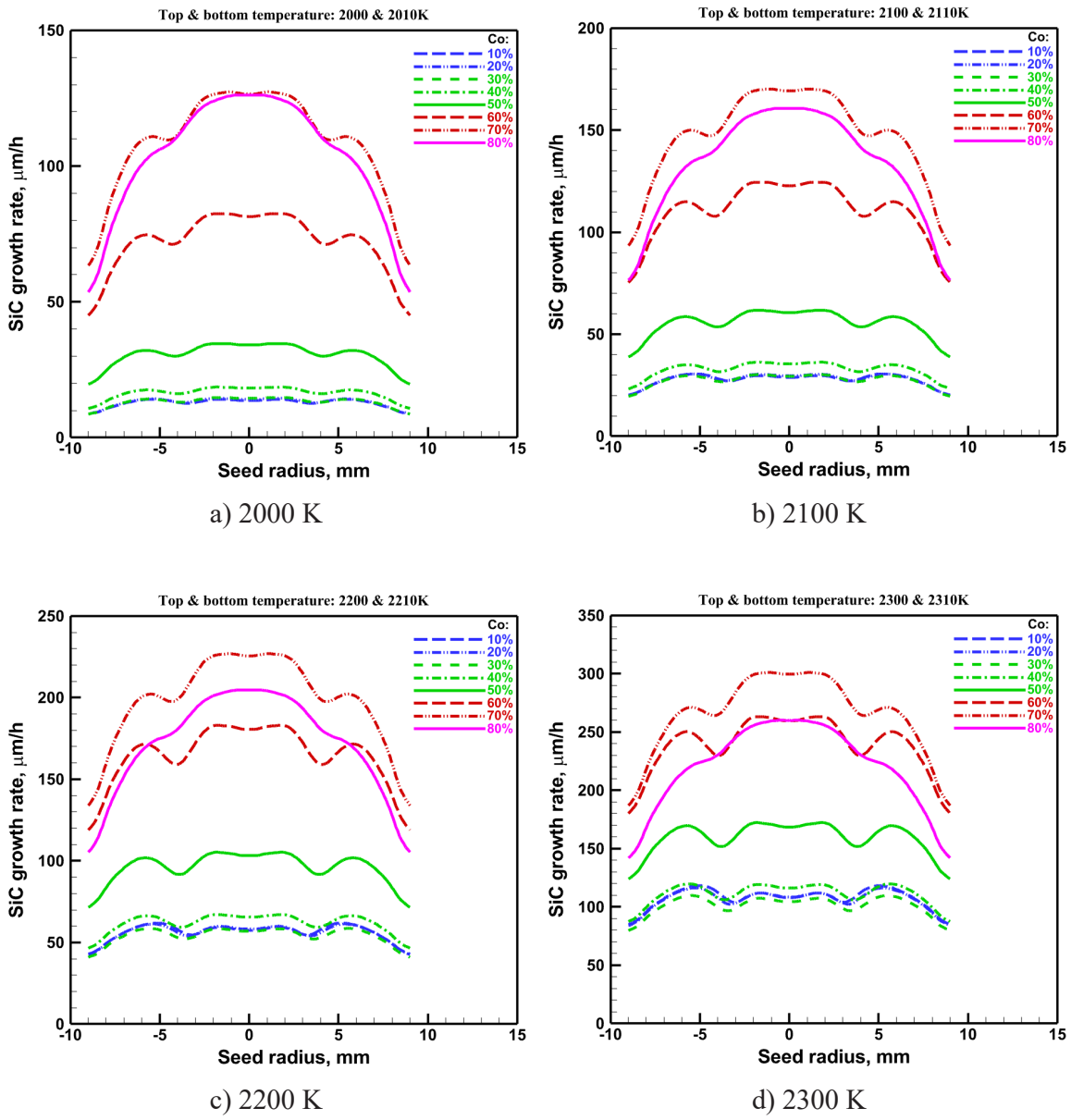

Fig. A4. Radial distribution of SiC growth rate at various Co-doping and seed top temperatures of a) 2000 K, b) 2100 K, c) 2200 K, and d) 2300 K.

Table A2. Characteristics of Si-Co solution: drop of temperature, carbon mass fraction over melt, maximum and averaged growth rate.

Si-Co solution	Temperatures controlled above seed and under bottom	
	2000 and 2010 K	2300 and 2310 K
20% Co	2011 – 2026 K; 0.74% $4.90 \cdot 10^{-4}$ – $5.03 \cdot 10^{-4}$; 2.59% 14.5 and 12.5 μm/h	2317 – 2340 K; 0.99% $3.09 \cdot 10^{-3}$ – $3.17 \cdot 10^{-3}$; 2.50% 116 and 104 μm/h
30% Co	2011 – 2026 K; 0.74% $5.34 \cdot 10^{-4}$ – $5.48 \cdot 10^{-4}$; 2.52% 14.8 and 12.6 μm/h	2317 – 2340 K; 0.99% $3.17 \cdot 10^{-3}$ – $3.25 \cdot 10^{-3}$; 2.40% 109 and 99 μm/h
40% Co	2011 – 2026 K; 0.74% $7.58 \cdot 10^{-4}$ – $7.76 \cdot 10^{-4}$; 2.36% 18.6 and 15.6 μm/h	2318 – 2339 K; 0.90% $3.97 \cdot 10^{-3}$ – $4.06 \cdot 10^{-3}$; 2.20% 120 and 109 μm/h
50% Co	2011 – 2026 K; 0.74% $1.73 \cdot 10^{-3}$ – $1.76 \cdot 10^{-3}$; 2.04% 34.6 and 28.8 μm/h	2318 – 2339 K; 0.90% $7.19 \cdot 10^{-3}$ – $7.32 \cdot 10^{-3}$; 1.82% 172 and 155 μm/h

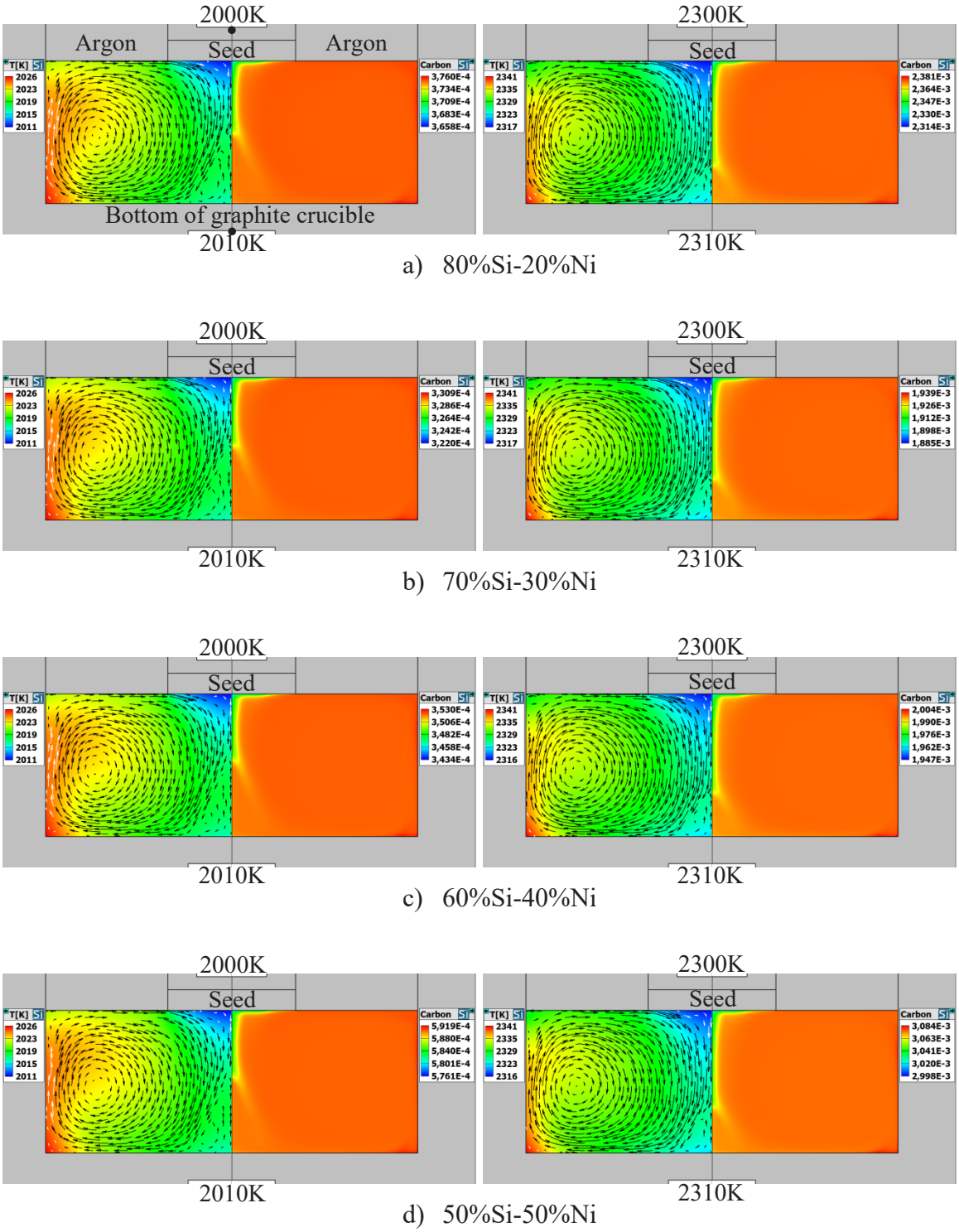

Fig. A5. 2D-distributions of temperature with velocity vectors and carbon mass fraction in Si-Ni solution of various composition. Temperatures shown at top and bottom of growth chamber are kept constant providing 10 K between these points.

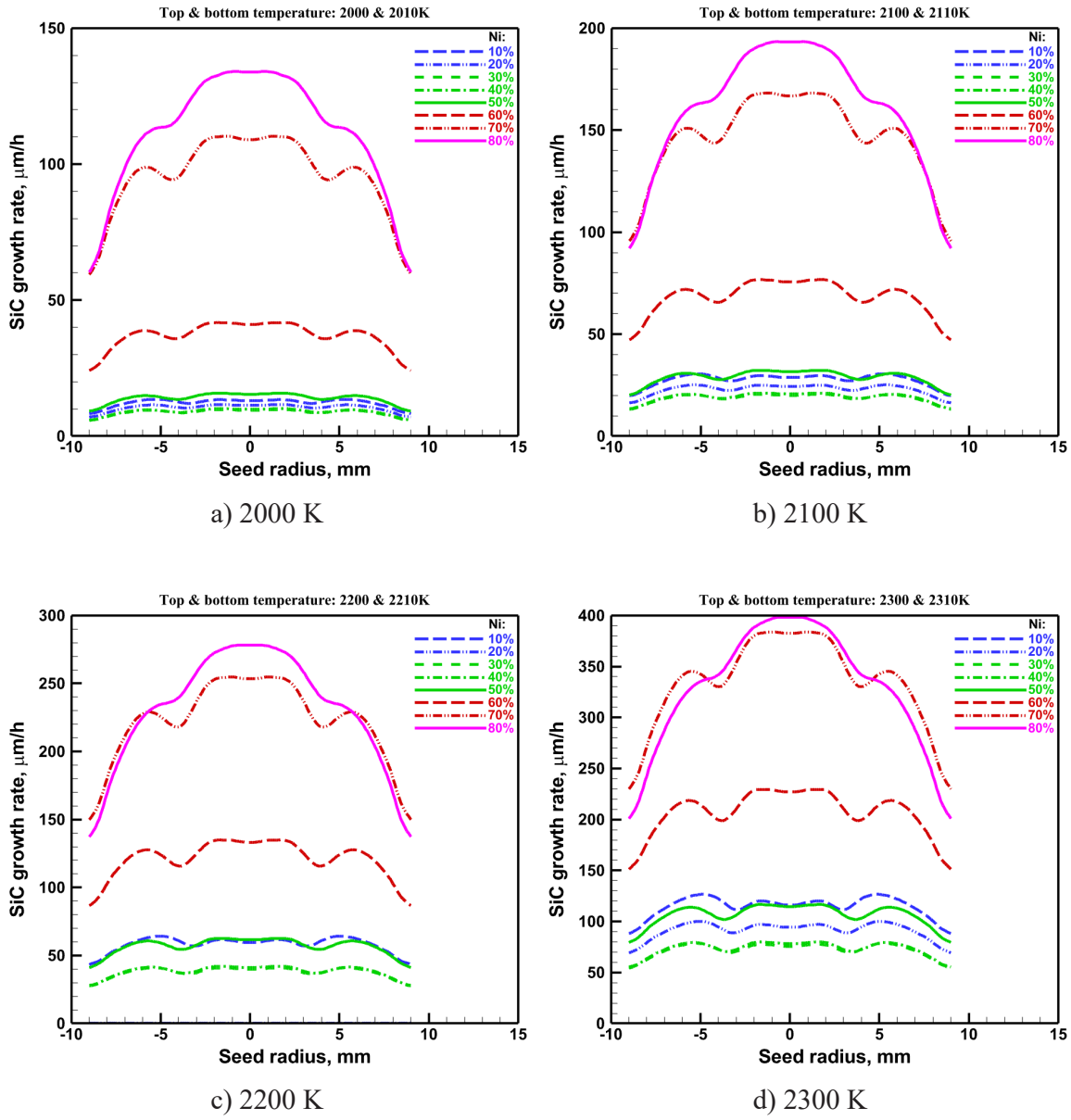

Fig. A6. Radial distribution of SiC growth rate at various Ni-doping and seed top temperatures of a) 2000 K, b) 2100 K, c) 2200 K, and d) 2300 K.

Table A3. Characteristics of Si-Ni solution: drop of temperature, carbon mass fraction over melt, maximum and averaged growth rate.

Si-Ni solution	Temperatures controlled above seed and under bottom	
	2000 and 2010 K	2300 and 2310 K
20% Ni	2011 – 2026 K; 0.74% $3.66 \cdot 10^{-4}$ – $3.76 \cdot 10^{-4}$; 2.72% 11.6 and 10.1 μm/h	2317 – 2341 K; 1.03% $2.31 \cdot 10^{-3}$ – $2.38 \cdot 10^{-3}$; 2.82% 100 and 88.9 μm/h
30% Ni	2011 – 2026 K; 0.74% $3.22 \cdot 10^{-4}$ – $3.31 \cdot 10^{-4}$; 2.70% 9.74 and 8.35 μm/h	2317 – 2341 K; 1.03% $1.88 \cdot 10^{-3}$ – $1.94 \cdot 10^{-3}$; 2.79% 78.6 and 70.0 μm/h
40% Ni	2011 – 2026 K; 0.74% $3.43 \cdot 10^{-4}$ – $3.53 \cdot 10^{-4}$; 2.73% 10.1 and 8.56 μm/h	2316 – 2341 K; 1.07% $1.95 \cdot 10^{-3}$ – $2.00 \cdot 10^{-3}$; 2.85% 79.7 and 71.1 μm/h
50% Ni	2011 – 2026 K; 0.74% $5.76 \cdot 10^{-4}$ – $5.92 \cdot 10^{-4}$; 2.68% 15.7 and 13.3 μm/h	2316 – 2341 K; 1.07% $3.00 \cdot 10^{-3}$ – $3.08 \cdot 10^{-3}$; 2.80% 116 and 103 μm/h

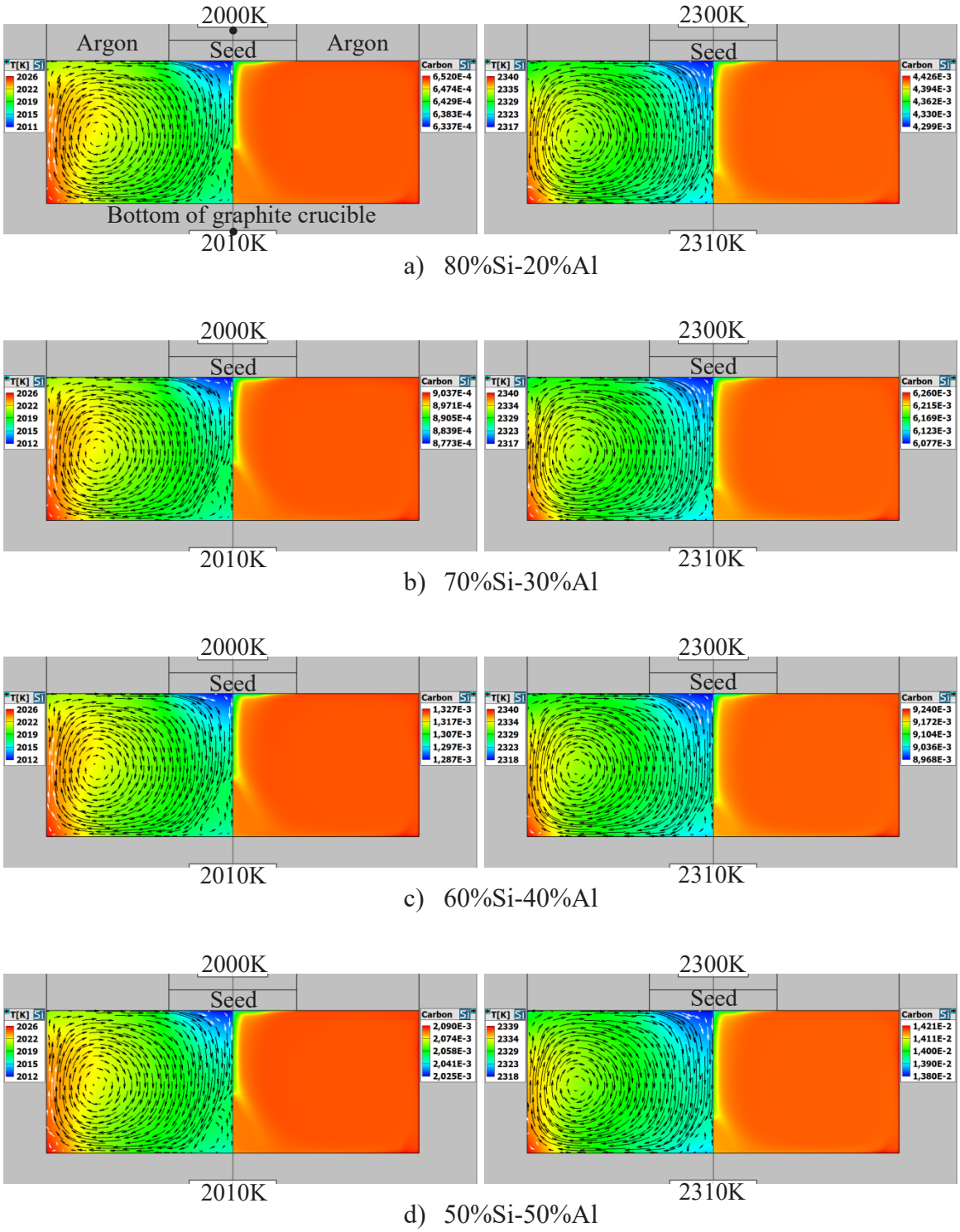

Fig. A7. 2D-distributions of temperature with velocity vectors and carbon mass fraction in Si-Al solution of various composition. Temperatures shown at top and bottom of growth chamber are kept constant providing 10 K between these points.

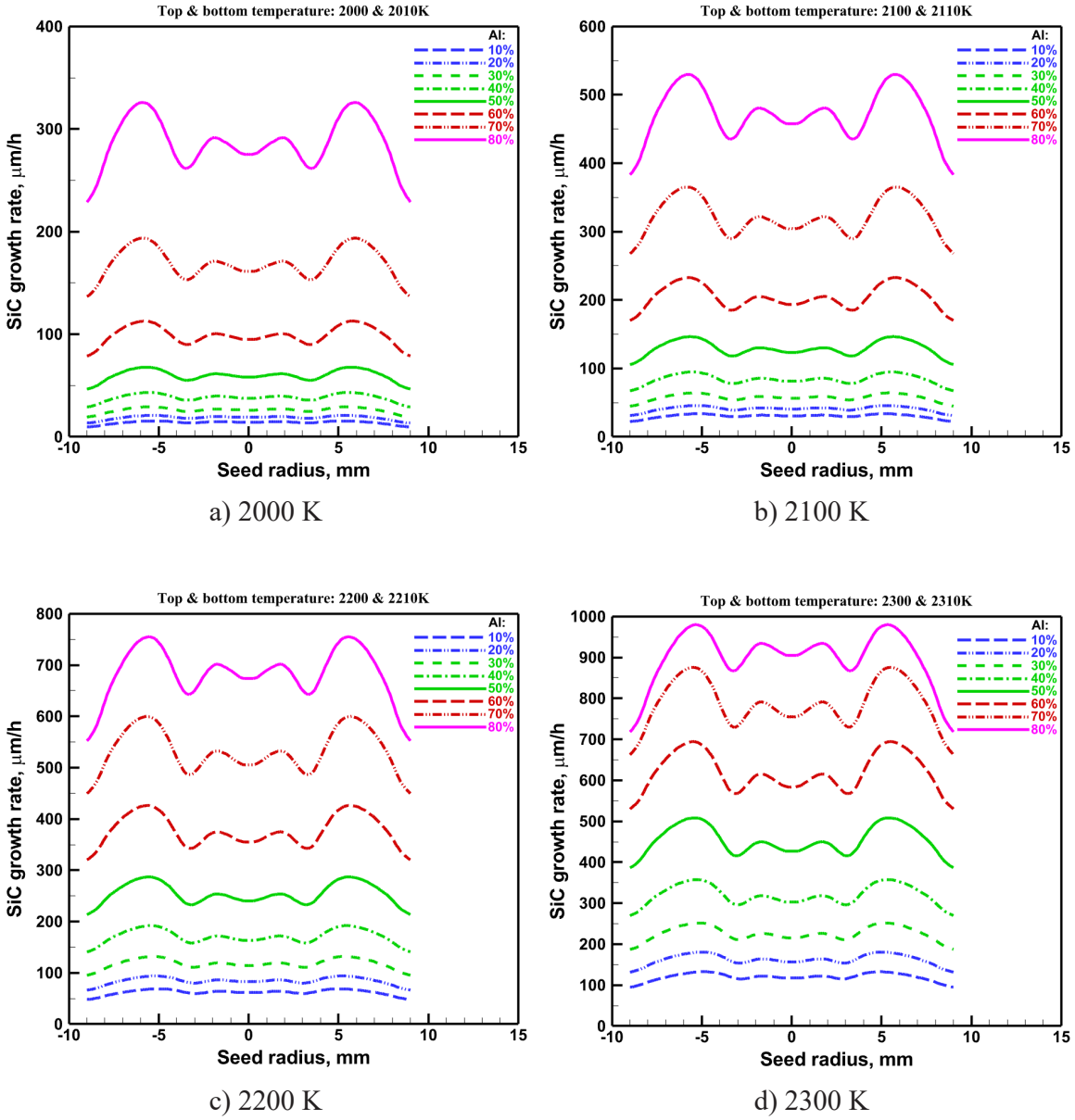

Fig. A8. Radial distribution of SiC growth rate at various Al-doping and seed top temperatures of a) 2000 K, b) 2100 K, c) 2200 K, and d) 2300 K.

Table A4. Characteristics of Si-Al solution: drop of temperature, carbon mass fraction over melt, maximum and averaged growth rate.

Si-Al solution	Temperatures controlled above seed and under bottom	
	2000 and 2010 K	2300 and 2310 K
20% Al	2011 – 2026 K; 0.74% $6.34 \cdot 10^{-4}$ – $6.52 \cdot 10^{-4}$; 2.81% 20.9 and 18.2 μm/h	2317 – 2340 K; 0.99% $4.30 \cdot 10^{-3}$ – $4.43 \cdot 10^{-3}$; 2.88% 180 and 161 μm/h
30% Al	2012 – 2026 K; 0.69% $8.77 \cdot 10^{-4}$ – $9.04 \cdot 10^{-4}$; 2.93% 29.2 and 25.6 μm/h	2317 – 2340 K; 0.99% $6.08 \cdot 10^{-3}$ – $6.26 \cdot 10^{-3}$; 2.93% 252 and 225 μm/h
40% Al	2012 – 2026 K; 0.69% $1.29 \cdot 10^{-3}$ – $1.33 \cdot 10^{-3}$; 3.02% 43.3 and 37.9 μm/h	2318 – 2340 K; 0.94% $8.97 \cdot 10^{-3}$ – $9.24 \cdot 10^{-3}$; 2.95% 358 and 321 μm/h
50% Al	2012 – 2026 K; 0.69% $2.02 \cdot 10^{-3}$ – $2.09 \cdot 10^{-3}$; 3.12% 68.0 and 59.6 μm/h	2318 – 2339 K; 0.90% $1.38 \cdot 10^{-2}$ – $1.42 \cdot 10^{-2}$; 2.89% 507 and 457 μm/h

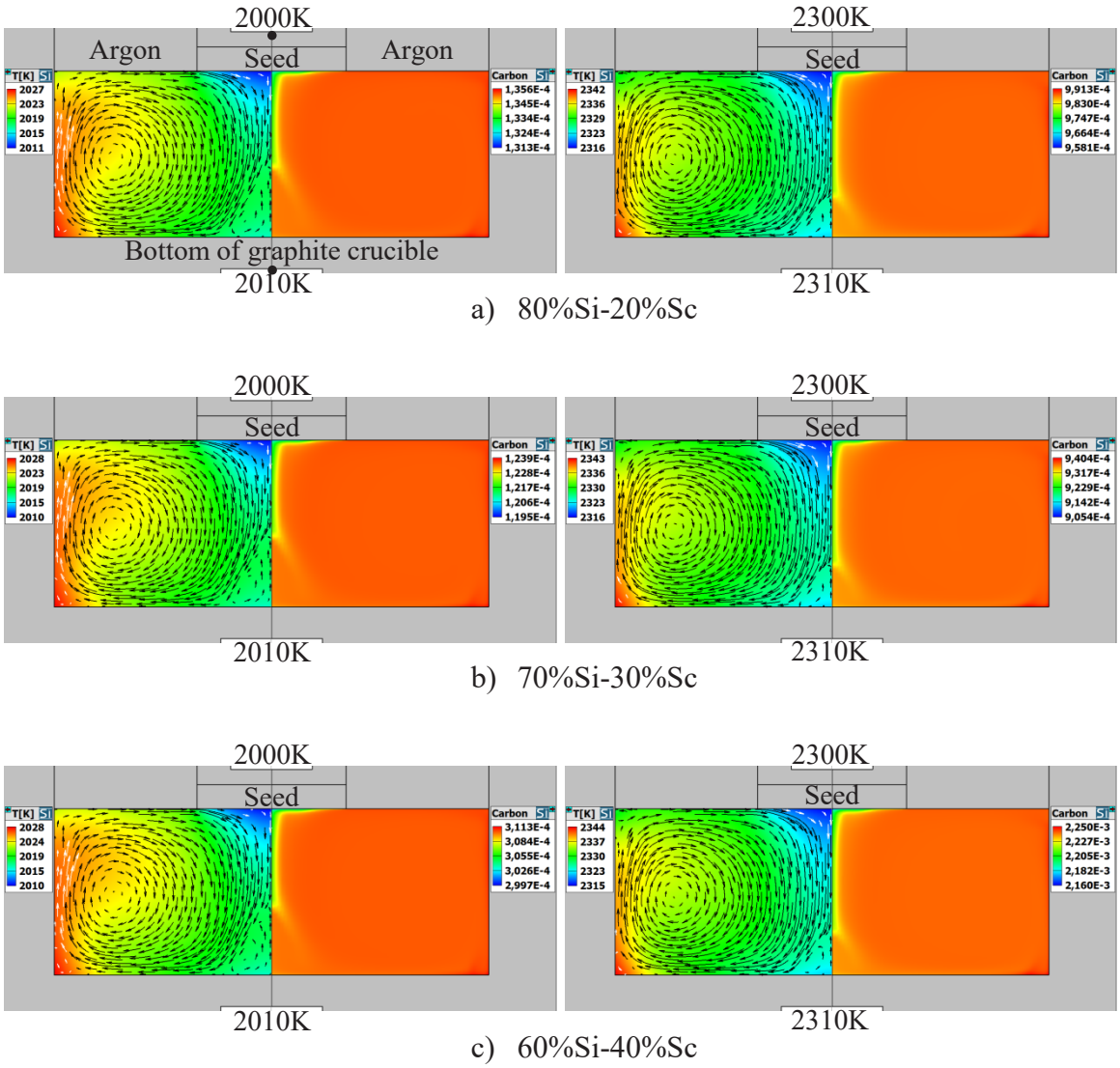

Fig. A9. 2D-distributions of temperature with velocity vectors and carbon mass fraction in Si-Sc solution of various composition. Temperatures shown at top and bottom of growth chamber are kept constant providing 10 K between these points.

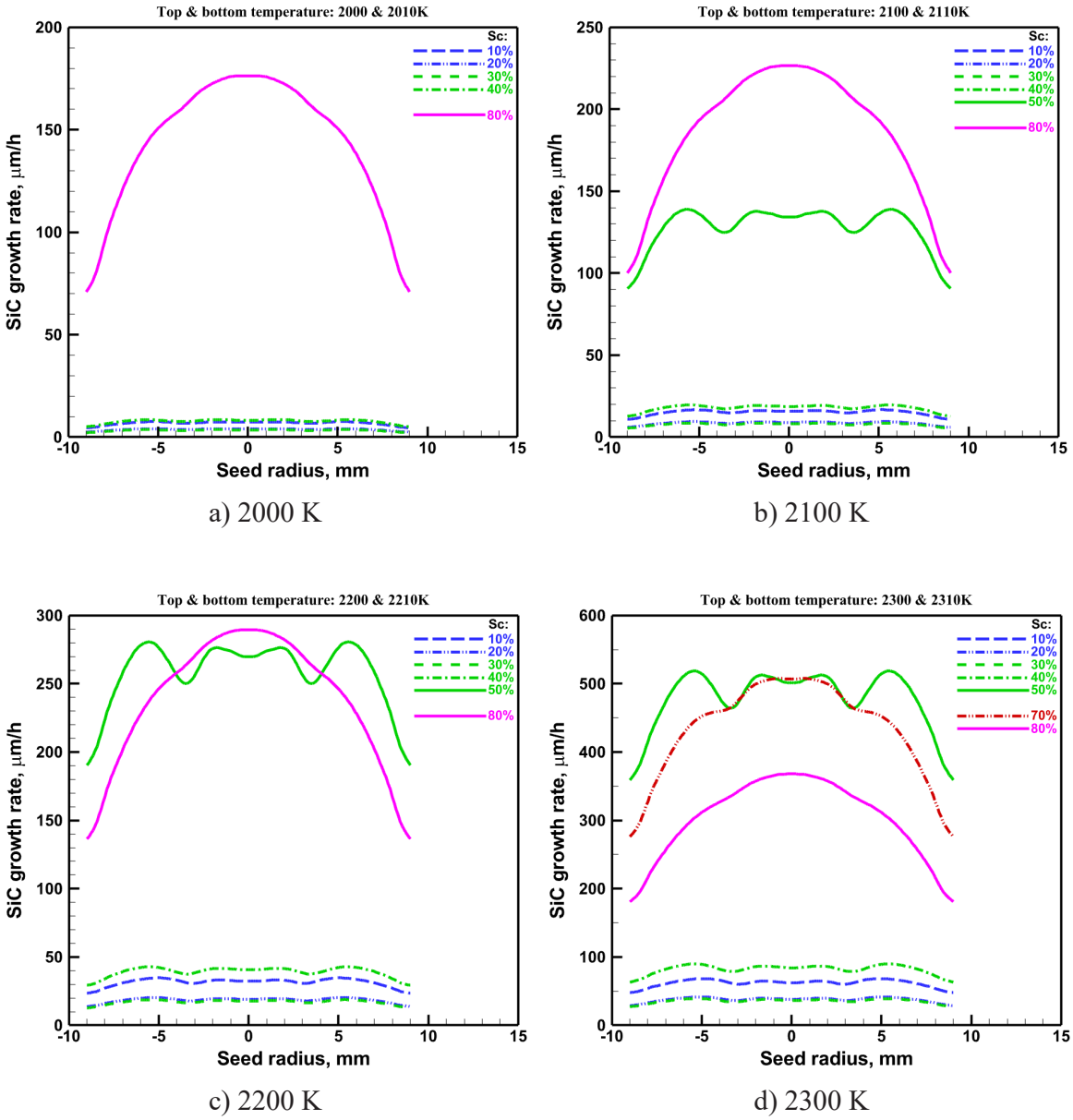

Fig. A10. Radial distribution of SiC growth rate at various Sc-doping and seed top temperatures of a) 2000 K, b) 2100 K, c) 2200 K, and d) 2300 K.

Table A5. Characteristics of Si-Sc solution: drop of temperature, carbon mass fraction over melt, maximum and averaged growth rate.

Si-Sc solution	Temperatures controlled above seed and under bottom	
	2000 and 2010 K	2300 and 2310 K
20% Sc	2011 – 2027 K; 0.79% $1.31 \cdot 10^{-4}$ – $1.36 \cdot 10^{-4}$; 3.18% 4.11 and 3.57 μm/h	2316 – 2342 K; 1.11% $9.58 \cdot 10^{-4}$ – $9.91 \cdot 10^{-4}$; 3.36% 41.4 and 36.7 μm/h
30% Sc	2010 – 2028 K; 0.89% $1.19 \cdot 10^{-4}$ – $1.24 \cdot 10^{-4}$; 3.56% 3.65 and 3.19 μm/h	2316 – 2343 K; 1.16% $9.05 \cdot 10^{-4}$ – $9.40 \cdot 10^{-4}$; 3.73% 39.2 and 34.8 μm/h
40% Sc	2010 – 2028 K; 0.89% $3.00 \cdot 10^{-4}$ – $3.11 \cdot 10^{-4}$; 3.74% 8.49 and 7.44 μm/h	2315 – 2344 K; 1.24% $2.16 \cdot 10^{-3}$ – $2.25 \cdot 10^{-3}$; 4.02% 89.7 and 80.2 μm/h
50% Sc	–	2315 – 2345 K; 1.28% $1.61 \cdot 10^{-2}$ – $1.67 \cdot 10^{-2}$; 3.61% 517 and 464 μm/h

REFERENCES

[1] A.N. Vorob'ev, Computational Analysis of SiC Crystal Growth from Silicon Melt Diluted with Cr, Fe, Co, Ni, Y, Al, La, Ce, Pr, Nd, and Sc. Part 1, *Reviews on Advanced Materials and Technologies*, 2024, vol. 6, no. 2, pp. 47–61.

[2] T. Kimoto, J.A. Cooper, *Fundamentals of silicon carbide technology: growth, characterization, devices and applications*, John Wiley & Sons Singapore Pte. Ltd: Singapore, 2014.

[3] Yu.M. Tairov, Growth of bulk SiC, *Materials Science and Engineering B*, 1995, vol. 29, no. 1–3, pp. 83–89.

[4] A.R. Powell, J.J. Sumakeris, Y. Khlebnikov, M.J. Paisley, R.T. Leonard, E. Deyneka, S. Gangwal, J. Ambati, V. Tsevtkov, J. Seaman, A. McClure, C. Horton, O. Kramarenko, V. Sakhalkar, M. O'Loughlin, A.A. Burk, J.Q. Guo, M. Dudley, E. Balkas, Bulk Growth of Large Area SiC Crystals, *Materials Science Forum*, 2016, vol. 858, pp. 5–10.

[5] H. Daikoku, M. Kado, H. Sakamoto, H. Suzuki, T. Bessho, K. Kusunoki, N. Yashiro, N. Okada, K. Moriguchi, K. Kamei, Top-Seeded Solution Growth of 4H-SiC Bulk Crystal Using Si-Cr Based Melt, *Materials Science Forum*, 2012, vol. 717–720, pp. 61–64.

[6] J.E. Lee, B.G. Kim, J.-Y. Yoon, M.-T. Ha, M.-H. Lee, Y. Kim, W.-S. Seo, H.-J. Choi, W.-J. Lee, S.-M. Jeong, The role of an SiC interlayer at a graphite-silicon liquid interface in the solution growth of SiC crystals, 2016, *Ceramics International*, vol. 42, no. 10, pp. 11611–11618.

[7] M.-T. Ha, Y.-J. Yu, Y.-J. Shin, S.-Y. Bae, M.-H. Lee, C.-J. Kim, S.-M. Jeong, Flow modification enhancing the growth rate in top seeded solution growth of SiC crystals, *RSC Advances*, 2019, vol. 9, no. 45, pp. 26327–26337.

[8] S. Harada, Y. Yamamoto, K. Seki, A. Horio, T. Mitsuhashi, M. Tagawa, T. Ujihara, Evolution of threading screw dislocation conversion during solution growth of 4H-SiC, *APL Materials*, 2013, vol. 1, no. 2, art. no. 022109.

[9] S. Xiao, S. Harada, K. Murayama, M. Tagawa, T. Ujihara, Conversion Behavior of Threading Screw Dislocations on C Face with Different Surface Morphology During 4H-SiC Solution Growth, *Crystal Growth and Design*, 2016, vol. 16, no. 11, pp. 6436–6439.

[10] F. Durand, J.C. Duby, Carbon solubility in solid and liquid silicon - A review with reference to eutectic equilibrium, *Journal of Phase Equilibria*, 1999, vol. 20, pp. 61–63.

[11] F. Mercier, J.-M. Dedulle, D. Chaussende, M. Pons, Coupled heat transfer and fluid dynamics modeling of high-temperature SiC solution growth, *Journal of Crystal Growth*, 2010, vol. 312, no. 2, pp. 155–163.

[12] F. Mercier, S. Nishizawa, Solution growth of SiC from silicon melts: Influence of the alternative magnetic field on fluid dynamics, *Journal of Crystal Growth*, 2011, vol. 318, no. 1, pp. 385–388.

[13] T. Narumi, S. Kawanishi, T. Yoshikawa, K. Kusunoki, K. Kamei, H. Daikoku, H. Sakamoto, Thermodynamic evaluation of the C-Cr-Si, C-Ti-Si, and C-Fe-Si systems for rapid solution growth of SiC, *Journal of Crystal Growth*, 2014, vol. 408, pp. 25–31.

[14] K. Kusunoki, K. Kamei, K. Seki, S. Harada, T. Ujihara, Nitrogen doping of 4H-SiC by the top-seeded solution growth technique using Si-Ti solvent, *Journal of Crystal Growth*, 2014, vol. 392, pp. 60–65.

[15] K. Kamei, K. Kusunoki, N. Yashiro, N. Okada, K. Moriguchi, H. Daikoku, M. Kado, H. Suzuki, H. Sakamoto, T. Bessho, Crystallinity Evaluation of 4H-SiC Single Crystal Grown by Solution Growth Technique Using Si-Ti-C Solution, *Materials Science Forum*, 2012, vol. 717–720, pp. 45–48.

[16] K. Kusunoki, N.Yashiro, N. Okada, K. Moriguchi, K. Kamei, M. Kado, H. Daikoku, H. Sakamoto, H. Suzuki, T. Bessho, Growth of large diameter 4H-SiC by TSSG technique, *Materials Science Forum*, 2013, vol. 740–742, pp. 65–68.

[17] Gq. Liang, H. Qian, Yl. Su, L. Shi, Q. Li, Y. Liu, Review of solution growth techniques for 4H-SiC single crystal, *China Foundry*, 2023, vol. 20, no. 2, pp. 159–178.

[18] *STR Group: official website*, URL: https://www.str-soft.com/ (last access: 10.11.2025).

[19] S. Bawazeer, A.A. Mohamad, P. Oclon, Natural convection in a differentially heated enclosure filled with low Prandtl number fluids with modified lattice Boltzmann method, *International Journal of Heat and Mass Transfer*, 2019, vol. 143, art. no. 118562.

[20] W. Chan, M.C. Gao, Ö.N. Doğan, P. King, A.D. Rollett, Thermodynamic assessment of Cr-Rare earth systems, *Journal of Phase Equilibria and Diffusion*, 2009, vol. 30, no. 6, pp. 578–586.

[21] S.-X. Wu, L. Wang, H.-P. Yuan, Q. Luo, Q. Li, K.-C. Chou, Experimental investigation and thermodynamic assessment of La–Y–Ni ternary system in Ni-rich corner, *Rare Metals*, 2023, vol. 42, no. 4, pp. 1316–1331.

УДК 538.91:539.374.1

Численный анализ роста карбида кремния из расплава кремния, разбавленного Cr, Fe, Co, Ni, Y, Al, La, Ce, Pr, Nd и Sc. Часть 2

А.Н. Воробьев[1,2]

[1] АО «ГРУППА СТР» – ООО «Софт-импакт», Большой Сампсониевский пр., 64 литера «Е», офис 603, Санкт-Петербург, 194044, Россия
[2] НПО «Стекло и керамика», ул. Дудко, 3, Санкт-Петербург, 192029, Россия

Аннотация. С учётом опыта, накопленного в предыдущей работе, численно проводится расширенный двухмерный анализ роста карбида кремния из 11 бинарных растворов в условиях, типичных для реального процесса, при температурах и составах, изменяющихся в широком диапазоне. Наряду с осреднёнными значениями скорости роста, исследуются её радиальные распределения по подложке для оценки формы поверхности растущего кристалла. Найдено, что за исключением алюминия добавление прочих присадок к расплаву кремния проявляется в насыщении скорости роста при их некотором уровне, выше которого скорость роста не увеличивается. Как следует из исследования радиального распределения, его отклонение от выпуклого параболического профиля уменьшается с возрастанием доли присадок и температуры. В этой связи, хром, лантаниды и иттрий могут быть выделены как наиболее перспективные. Показано, что такие тройные растворы, как Si-Cr-Y и Si-La-Y, способны обеспечить одновременно относительно высокую скорость роста и близкую к параболической поверхность кристалла при умеренном содержании легирующей примеси.

Ключевые слова: рост карбида кремния; расплав кремния; раствор; растворимость углерода; МРК (моделирование роста кристаллов)